# Temporally Adaptive Conditioned Responses: Representation of the Stimulus Trace in Neural-Network Models

John E. Desmond

COINS Technical Report 88-80
October 14, 1988

University of Massachusetts
Amherst, Massachusetts 01003

## Summary

Theories of classical (Pavlovian) conditioning and neural-network approaches to learning share a common goal of understanding how connections between events develop and are transformed into adaptive behavior. Computational models of conditioning are therefore relevant to neural-network and adaptive control research.

Conditioned responses reflect not only knowledge of associations among events, but also reflect knowledge about the timing of these events. This is evident in two basic phenomena:

**Interstimulus interval phenomena.** Some CS–US interstimulus intervals are more effective than others in establishing a CS–US association.

**CR timing phenomena.** CRs are initiated prior to the US onset and tend to peak at the time of US occurrence. If the CS–US interval is changed, the timing of the CR adapts to the new interval.

Modeling both of these temporal phenomena is the subject of this report. The general approach taken is to computationally define a *stimulus trace*, a CS-evoked process to which theorists have attributed these temporal phenomena, and incorporate the stimulus trace in models of conditioning. The simplest such model, one using a single adaptive processing unit, is introduced in Section 1, and the limitations of this approach are discussed. Section 2 addresses these limitations by re-defining the stimulus trace and introducing a network approach to modeling CR timing. In Section 3, the stimulus trace of Section 2 is extended to account for both stimulus timing and response timing phenomena.

## Contents

# 1. Introduction

Many biological systems learn to associate two events, but such an association is often insufficient for generating adaptive responses unless the timing of the two events is also learned. For example, consider a traffic light that has just changed from green to yellow. The expectation of when the light will turn red, acquired through repeated experience with traffic lights, allows the driver to react appropriately, i.e., slow down or speed up. The light changing from yellow to red evokes a different temporal expectation for when it will change again to green. Note that it is more difficult to predict when the light will turn green from the red onset than it is to predict when it will turn red from the yellow onset. This is because the yellow-to-red *interstimulus interval* is far more effective than the longer red-to-green interval for learning temporal relationships and generating adaptive behavior.

How the timing of events affects both the associability of the events and the timing of the adaptive response have been central issues in classical conditioning ever since Pavlov's initial description of the conditional response. Computational models of conditioning have begun to address these issues. However, returning to the traffic light example, most of these models are capable of learning the yellow-red association but not the timing information that allows the association to become an adaptive response.

This report addresses from a connectionist and learning-theoretical perspective how temporal expectations of events are developed, how the temporal separation of events influences the robustness of these expectations, and how these expectations are expressed in the conditioned response waveform. These issues are relevant to an understanding of more complex motor behavior; such behavior can be regarded as a sequence of elemental motor responses that are executed at the appropriate times. It is hoped that the timing of such elemental responses will be illuminated by investigating perhaps the most basic form of adaptive timing, the conditioned response.

## 1.1 Background

Models of classical conditioning can describe learning phenomena at different levels of detail. For example, a model can focus on phenomena that occur from one trial to the next, a trial being defined as a single presentation of the stimulus events involved in the training protocol. Such a model, referred to as a *trial-level* model, describes conditioning by showing the changes in connection strength between the conditioned (CS) and unconditioned (US) stimuli that occur over trials. The Rescorla-Wagner model (Rescorla and Wagner, 1972) is one such trial-level model that successfully predicts the outcome of many conditioning

protocols. For example, in acquisition training, in which the neutral CS is first paired with the non-neutral US, the Rescorla-Wagner model predicts that the CS–US associative strength increases over trials to an asymptotic level. If the US is subsequently removed and CS-alone trials are presented (i.e., extinction training), the model predicts that associative strength decreases over trials.

In recent years, theorists have begun to focus not only on the events that occur across trials but also those that occur within trials, and this has resulted in a class of so-called *real-time* models of conditioning. These models address the role that the temporal relationships among stimuli have in the development of associations.[1] For example, real-time models can accurately predict that acquisition training with "forward pairing" of the stimuli, in which the CS precedes the US, is a much more effective means of forming an association than "backward pairing." These models also accurately predict that the effectiveness of forward pairing depends on the CS–US interstimulus interval. Predictions of stimulus timing effects such as these are possible for real-time models but not for trial-level models.

Although all real-time models address the timing of the *stimuli* in conditioning, few address the timing (i.e., topography) of the conditioned response (CR). For example, CRs generated by animals can be characterized by features such as onset latency, peak amplitude, time of peak, number of peaks, total duration, etc. If a real-time model is to accurately portray conditioning, these features of CRs should be generated in the model's output. What is to be gained by such a detailed treatment of conditioning? Inspection of CR waveforms suggests that *temporal expectations* develop as CS–US associations develop. For example, the waveform of the CR is typically such that the peak amplitude occurs at the temporal locus of the US. Changing the CS–US timing produces corresponding changes in the CR waveform (e.g., Coleman and Gormezano, 1971; Gormezano, 1972; Gormezano et al., 1983; Millenson et al., 1977; Pavlov, 1927; Schneiderman and Gormezano, 1964; Schneiderman, 1966; Smith, 1968). Thus, when an animal receives a CS presentation, the animal expresses knowledge of *what* to expect by generating a CR from the appropriate response system, and it expresses knowledge of *when* to expect it by executing the response at the appropriate time. Both of these aspects of learning are essential for generating adaptive behavior. Modeling CR topography, therefore, is an appropriate way to study the formation of temporal expectations, particularly when the predictions of the model can be tested experimentally.

---

[1]Some of the recent real-time approaches to modeling classical conditioning include: Barto and Sutton, 1982; Desmond and Moore, 1988; Gelperin et al., 1985; Gluck and Thompson, 1987; Grossberg and Schmajuk, 1987; Klopf, 1988; Levine, 1986; Moore et al., 1986; Schmajuk and Moore, 1985, 1988; Sutton and Barto, 1981; Tesauro, 1986; Wagner, 1981.

This report focuses on real-time approaches to modeling that include trial-level phenomena, stimulus timing effects, and the timing of the response. In so doing, this report incorporates some notions from learning theory within a computational connectionist framework. In particular, the stimulus trace, a process to which theorists have attributed both stimulus and response timing properties, is included in the design of the models. Section 1.1 describes a simple method for modeling the stimulus trace; this approach uses the most basic neural model architecture, that of a single adaptive processing unit. The section ends with a discussion of the problems and limitations of this approach. Section 2 begins to address these limitations by re-defining the stimulus trace mechanism and presenting a network that successfully models CR topography. Section 3 proposes a method by which the stimulus trace of Section 2 can be extended to account for the effects of stimulus timing as well as for the timing of the CR.

## 1.2 The stimulus trace

The concept of the stimulus trace in classical conditioning was postulated by Pavlov (1927) to account for the fact that the CS does not have to be explicitly present for the CR to occur. One of the conditioning protocols used by Pavlov, now referred to as "trace conditioning," entails the US onset occurring after the CS offset. The presence of a CR within the "trace interval," the time between CS offset and US onset, suggested to Pavlov that a neural trace, initiated by the CS, was responsible for CR generation.

Subsequent theorists have built on Pavlov's stimulus trace notion, and have used the trace to account for classical conditioning phenomena. One phenomenon that has been explained by the trace hypothesis is that the rate of conditioning varies depending on the interval of time between CS onset and US onset.[2] This observation led to the hypothesis that *the CS initiates a trace that changes in strength over time, and the rate of learning is proportional to the strength of the trace at the time the reinforcement is delivered* (Gormezano, 1972; Hull, 1943). Experimental studies sought to characterize the time course of the stimulus trace by carefully measuring the rate of conditioning as a function of ISI. From these experiments it was deduced that *the strength of the trace is a non-monotonic, inverted U-shaped function of time, with the peak occurring at some optimal interstimulus interval.*[3]

---

[2] As indicated above, this interval is referred to as the CS–US interstimulus interval, or ISI for short. Reference to "ISI effects" or "ISI phenomena" below refers to the fact that the ISI influences the rate of learning.

[3] These experiments addressed the issue of whether the same ISI function existed for all types of CRs. The results of these studies indicated that the ISI function varies considerably depending on the response

Another phenomenon that has been linked to the stimulus trace is that CRs tend to anticipate the US onset, with the amount of anticipation increasing over training. Hence, in addition to Pavlov's implicit assumption that *the stimulus trace provides the driving force for the CR*, theorists have also proposed that *the strength of the CR is proportional to the strength of the trace*, and that anticipatory CRs occur when *earlier weaker portions of the trace become capable of eliciting the response* (Gormezano, 1972; Hull, 1943; 1952).

Thus, theorists have attributed to the stimulus trace the ability to influence learning based on the timing of the stimuli and the ability to generate anticipatory responses. Can a stimulus trace with both of these properties be incorporated into a real-time model, and would such a trace produce realistic conditioning simulations? To begin answering this question it is necessary to introduce the basic approach taken by a number of modelers, which is that conditioning phenomena can be modeled using a single "adaptive processing unit," such as that illustrated in Figure 1.[4] The term "processing unit" means that the unit's output is computed on the basis of its inputs; the "adaptive" part refers to the fact that the unit's output to an input can change.[5] In the figure, CS and US inputs are depicted as converging on the unit. CS inputs are denoted by $I_i(t)$, where the subscript $i$ denotes the fact that a number of different CSs may be present. The US input is denoted by $\lambda(t)$. $I_i(t)$ and $\lambda(t)$ take on values of 1 or 0 to denote "stimulus on" or "stimulus off," i.e., $I_i(t) = 1$ when $CS_i$ is on, $I_i(t) = 0$ when $CS_i$ is off, $\lambda(t) = 1$ when US is on, $\lambda(t) = 0$ when US is off.[6]

Through repeated pairings of $CS_i$ with the US, associative strength, $V_i(t)$, develops allowing $CS_i$ input to be transformed into CR output, $s(t)$. Associative strength, which is also referred to as connection strength, changes via the operation of an appropriate learning

---

system being measured (see Gormezano and Moore, 1969). The behavior of the models presented in this report are typically compared to that of the rabbit conditioned nictitating membrane response. The optimal interstimulus interval for this behavioral preparation is about 250 ms (Gormezano, Kehoe, and Marshall, 1983; Schneiderman, 1966; Schneiderman and Gormezano, 1964; Smith, 1968).

[4] Modeling both properties of the stimulus trace within a single-unit real-time framework was the approach taken by Moore et al. (1986) and is also described by Moore and Blazis (in press).

[5] In this report, "unit" implies an adaptive processing unit. In the next section, both units and "elements" are discussed. The latter term refers to a non-adaptive processing unit, i.e., the output of an element to a given set of inputs is always the same.

[6] Because Figure 1 represents a real-time approach to modeling CRs, the mathematical terms for the stimuli, response, and associative strength are all a function of time, $t$. In order to capture real-time properties of CR waveforms in computer simulations, time must be divided into arbitrarily small steps. In the simulations that are presented below, each step corresponds to a 10 ms epoch. Each trial begins at time $t = 1$, and $t$ is incremented until all stimuli have been presented and all responses have returned to baseline. The total number of time steps per trial, therefore, depends on the particular conditioning protocol involved and the duration of the stimuli.

rule. The rules discussed in this report can be described as "Hebb-like," because they are consistent with Hebb's hypothesis that when one neuron takes part in the excitation of a second neuron, the first neuron's efficiency in firing the second neuron increases (Hebb, 1949). This change in efficiency presumably occurs through metabolic changes in the synapse between the first and second cell. Thus, associative or connection strength is also referred to as *synaptic* strength or synaptic weight.

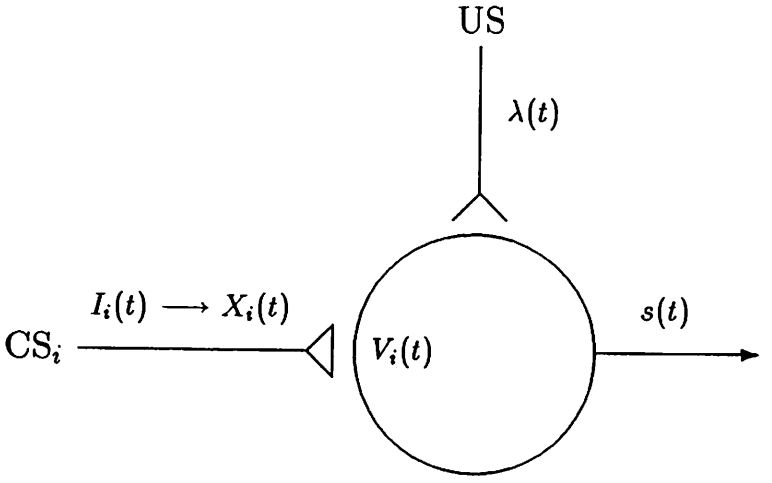


**Figure 1:** An adaptive processing unit for a simple real-time model of conditioning. The $CS_i$ signal, $I_i(t)$ is transformed into a stimulus trace, $X_i(t)$. A stimulus trace initially has no effect on the unit's output, $s(t)$. However, convergence of a trace with the US input, $\lambda(t)$, leads to changes in the connection or "synaptic" weight, $V_i(t)$, and these changes allow the stimulus traces to generate output from the unit. The output is a function of the stimulus traces, the synaptic weights, and the US, i.e., $s(t) = \sum V_i(t)X_i(t) + \lambda(t)$. In this and subsequent figures, open synaptic terminals ( -< ) represent non-modifiable connections, whereas closed terminals ( -◁ ) represent modifiable connections. In general, $n$ different CSs may converge on the unit, and the subscript $i$, where $i = 1, \ldots, n$, is used to denote this fact.

Figure 1 indicates that $CS_i$ input $I_i(t)$ initiates $X_i(t)$, the stimulus trace. From a biological perspective, $X_i(t)$ is some neuronal transformation of the stimulus energy provided by $CS_i$. The theoretical time course for $X_i(t)$ is given in Figure 2. Based on the assumptions outlined above for the stimulus trace, $X_i(t)$ performs two tasks, the first of which is to govern the rate of learning at a given ISI. One way to accomplish the rate-governing task is to allow $X_i(t)$ to regulate changes in associative strength. Thus, in this simple model, the $X_i(t)$ term is defined as an inverted U-shaped function that peaks at some optimal ISI (in accordance with empirical observations), and is present in the learning rule as a

weighting factor for changes in $V_i(t)$, i.e.,

$$\Delta V_i(t) = F(t)X_i(t) \tag{1}$$

where $F(t)$ represents a learning rule function, and is discussed below. The main point of Equation (1) is that when the stimulus trace is weak [i.e., $X_i(t) \approx 0$] there can be little change in associative strength. When the stimulus trace is strongest at the optimal ISI, changes in $V_i(t)$ are greatest.

The second task performed by $X_i(t)$ is to provide the driving force for the CR. A straightforward way to accomplish this task is to have the shape of $X_i(t)$ represent the waveform of a fully developed CR. However, because CR output is expressed only if associative strength between the CS and US develops, the model's output rule must reflect the contributions of both the trace and the associative strength. An output rule that satisfies this requirement is:

$$s(t) = \begin{cases} \sum V_i(t)X_i(t) + \lambda(t) & \text{if } \sum V_i(t)X_i(t) + \lambda(t) > \theta \\ \theta & \text{otherwise,} \end{cases} \tag{2}$$

where $\theta$ is a baseline response threshold. The net effect of Equation (2) on CR topography is described by Figure 3. As associative strength increases, an observable CR emerges as if the response threshold was being lowered. Note that CR onset latency decreases as associative strength increases, a phenomenon typically observed in experimental studies of classical conditioning.

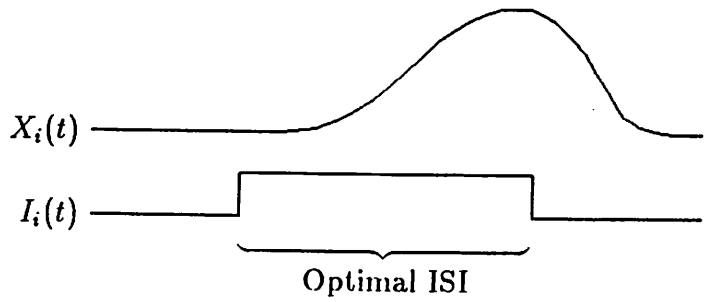


**Figure 2:** The relationship between $I_i(t)$, the $CS_i$ signal, and $X_i(t)$, the stimulus trace. The peak value of $X_i(t)$ is assumed to occur at the optimal ISI.

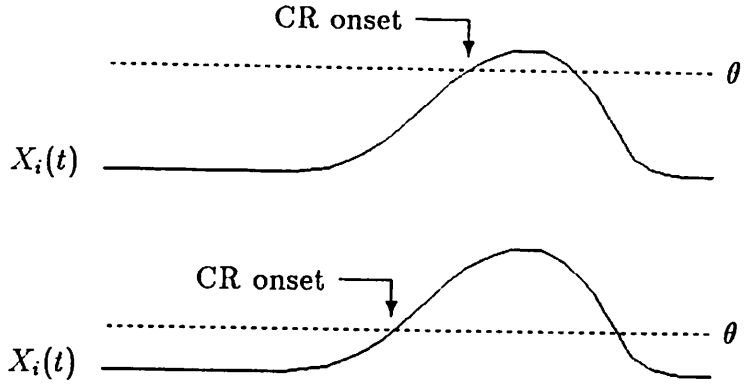


**Figure 3:** CR topography from a single adaptive processing unit at early stages of acquisition when $V_i(t)$ is small (upper trace), and at later stages when $V_i(t)$ is larger (lower trace). The CR is only what appears above the threshold level, $\theta$ (represented by the horizontal dotted line). Incrementing the synaptic weight $V_i(t)$ is analogous to lowering the threshold level and thereby allowing more of $X_i(t)$ to emerge into an observable CR.

### 1.3 Limitations of the single-unit approach

Equations (1) and (2) are mathematical statements of the properties ascribed to the stimulus trace. However, attempting to implement these equations in a model that (a) is a real-time model, (b) uses a single adaptive processing unit, and (c) generates CR topography, reveals problems and limitations which, as discussed in Section 2, can be addressed by using more than one adaptive processing unit.

One problem is choosing a suitable $F(t)$ for Equation (1). Consider first Hebb's (1949) rule,

$$\Delta V_i(t) = c\ s(t) X_i(t) \tag{1a}$$

where $c$ is a learning-rate constant. In this equation, $F(t) = c\ s(t)$. Although Hebb's rule was a significant first step for neural modeling, it does not lead to accurate predictions. For example, although the equation allows for increments in $V_i(t)$ and thereby simulates the acquisition of learning, negative values of $\Delta V_i(t)$ are not possible, and therefore, extinction and conditioned inhibition cannot be simulated.

In contrast, an alternative form of Equation (1), the so-called *least mean square (LMS) rule* (e.g., Gluck and Bower, 1988), allows for both positive and negative changes in $V_i(t)$.

It is written as follows:

$$\Delta V_i(t) = c[\lambda(t) - \hat{s}(t)]X_i(t) \tag{1b}$$

where $\hat{s}(t) = \sum V_i(t)X_i(t)$ and $F(t) = c[\lambda(t) - \hat{s}(t)]$. Equation (1b) is a "supervised" learning rule in which $\lambda(t)$ acts a specialized "teaching" input that controls the increments or decrements in weights. Sutton and Barto (1981) point out that Equation (1b) is a time-dependent version of the rule used by Rescorla and Wagner (1972). Although the rule used by Rescorla and Wagner (1972) is suitable for simulating across-trial conditioning phenomena, the rule represented by Equation (1b) is not as effective for real-time modeling of CR topography in a single adaptive processing unit. This is because the update of $V_i(t)$ at every time step can prevent any significant build-up of $V_i(t)$ over trials. For example, in simple acquisition training, increments in weight are quickly neutralized because the number of time steps in which the US is absent greatly exceeds the number of time steps in which the US is present, at least for any realistic simulation of classical conditioning in which time is divided into relatively small steps. Consequently, with Equation (1b), increments in $V_i(t)$ that occur when $\Delta V_i(t) = c[1 - \hat{s}(t)]X_i(t)$ are outnumbered by the decrements that occur when $\Delta V_i(t) = c[0 - \hat{s}(t)]X_i(t)$.

The continual update of $V_i(t)$ can also pose problems for learning rules that do not require a special teaching input. For example, consider an equation similar to that used by Sutton and Barto (1981) in which $F(t) = c[s(t) - \bar{s}(t)]$, and thus, the complete learning rule is

$$\Delta V_i(t) = c[s(t) - \bar{s}(t)]X_i(t) \tag{1c}$$

where $\bar{s}(t)$ is the expected output of the unit [equal to $s(t-1)$ in the simplest case]. In this equation, $V_i(t)$ will change at any time step $t$ in which $s(t) \neq \bar{s}(t)$. In the original Sutton and Barto model (1981), CS inputs are rectangular pulses [identical to $I_i(t)$ in Figure 2]; thus, $s(t)$ is also rectangular [by Equation (2)] and changes in $V_i(t)$ occur only when a CS or US goes on or off. However, if the CS input is a gradually changing function of time, such as $X_i(t)$, $\Delta V_i(t)$ may be nonzero at every time $t$ for which $X_i(t)$ is defined. Consequently, changes in $V_i(t)$ that occur *within* a trial are highly sensitive to the rate at which $X_i(t)$ rises and falls. Undesirable side effects such as "blow-up" of $V_i(t)$ can occur if increments in $V_i(t)$ that occur during the rising phase of $X_i(t)$ are not matched by decrements in $V_i(t)$ during the falling phase (an example of the blow-up tendency is illustrated in Table 1).

One way to change Equation (1c) and thereby avoid weight blow-up is to incorporate a second trace in the calculation of $\Delta V_i(t)$. Sutton and Barto (1981) make a distinction

| $t$ | $V_i(t)$ | $X_i(t)$ | $s(t)$ | $\bar{s}(t)$ | $s(t) - \bar{s}(t)$ | $[s(t) - \bar{s}(t)]X_i(t)$ |
|---|---|---|---|---|---|---|
| 1 | 0.500 | 0.000 | 0.000 | 0.000 | 0.000 | 0.000 |
| 2 | 0.500 | 0.500 | 0.250 | 0.000 | 0.250 | 0.125 |
| 3 | 0.625 | 1.000 | 0.625 | 0.250 | 0.375 | 0.375 |
| 4 | 1.000 | 0.500 | 0.500 | 0.625 | -0.125 | -0.063 |
| 5 | 0.938 | 0.000 | 0.000 | 0.500 | -0.500 | 0.000 |
| | 0.938 | $\Leftarrow$ Final $V_i(t)$ | | | | |

**Table 1:** An example of the tendency for $V_i(t)$ to "blow-up" using Equation (1c). The trial in this example consists of 5 time steps. The CS is assumed to go on at time $t = 1$ (only one CS is presented, so $i = 1$). $X_i(t)$ is defined as a simple rising and falling function. $V_i(t)$ is assumed to have a starting value of 0.5 at time $t = 1$; on subsequent time steps $V_i(t)$ is calculated using Equation (1c). The value for $s(t)$ is calculated using Equation (2), and $\bar{s}(t) = s(t-1)$. The table shows that, *without any US input*, $V_i(t)$ increases to 0.938 by the end of the trial. This tendency for blow-up can be avoided by using a second "eligibility" trace [i.e., $\bar{x}_i(t)$, after Sutton and Barto (1981)] in the learning rule rather than $X_i(t)$ (Moore et al., 1986).

between stimulating traces, which are capable of producing output from the adaptive unit, and nonstimulating traces, which do not produce output. In their model, a nonstimulating trace, referred to as an "eligibility trace" (see also Klopf, 1972), governs the rate of learning. Their learning rule, which differs from the general form of Equation (1), is:

$$\Delta V_i(t) = [s(t) - \bar{s}(t)]\bar{x}_i(t) \tag{3}$$

where $\bar{x}_i(t)$ is the eligibility of synapse $i$. Moore et al. (1986) demonstrated that Equation (3) can be successfully used in a model of CR topography, and that such a model retains the ability of the Sutton-Barto model to predict phenomena such as blocking, conditioned inhibition, and higher-order conditioning. However, the performance of the Moore et al. (1986) model is sensitive to changes in parameters (Blazis and Moore, 1987). For example, changing the rate of rise in $X_i(t)$ can alter the predicted ISI curve, or altering $\bar{x}_i(t)$ can change CR topography.

Regardless of the learning rule employed, single-unit models of topography can encounter additional problems when a stimulus trace of fixed time course [such as $X_i(t)$] is used in the CR-generation rule. For example, if in accordance with the assumptions outlined above, the magnitude of the stimulus trace peaks at the optimal ISI and subsequently declines, then the predicted CR topography resulting from a CS–US interval that is greater than the optimal ISI should look like the one in the top panel of Figure 4. The

simulated CR peaks and begins to fall prior to the US onset. However, this predicted waveform is generally *not* observed in experimental studies: the CR typically blends with the UR. If the assumptions of the stimulus trace are modified so that the trace begins to fall only after offset of the CS (Moore et al., 1986), the CR will once again blend with the UR, as depicted in the middle panel of Figure 4. However, this solution is unsatisfactory for two reasons: (a) The CR topography depicted in the middle panel of Figure 4 is not an accurate depiction of actual CR profiles observed at long CS–US intervals. Specifically, CRs at longer CS–US intervals tend to have a delayed onset, a phenomenon known as Pavlovian *inhibition of delay.*[7] (b) CRs in trace conditioning protocols are inaccurately predicted, as illustrated in the bottom panel of Figure 4. A realistic simulation of trace conditioning would show the CR rising within the trace interval and peaking at the time of US occurrence.

In summary, this section began with a description of two properties that have been attributed to the stimulus trace: the ability to generate anticipatory CRs, and the ability to govern the rate of learning at a given ISI. A straightforward way to model these properties is to incorporate a stimulus trace function, $X_i(t)$, into appropriate model equations [Equations (1) and (2)]. However, one can make the following observations concerning the use of this approach within a single-unit framework: (a) Using the conceptual scheme represented in Figures 1 and 2 and Equations (1) and (2), the continual update of $V_i(t)$ can pose problems for some of the currently used learning rules. Although the above discussion did not exhaustively review different learning rules, the main point is that learning rules that are stable and predictable when $X_i(t)$ is a binary signal and CR topography is not the target output can become unpredictable or can produce undesired behavior when $X_i(t)$ is made into an analog signal and CR topography is the target output. (b) Although it is parsimonius to assume a single trace mechanism for modeling classical conditioning phenomena, using one function to generate both properties of the stimulus trace can result in inappropriate predictions of CR topography, as seen in Figure 4. This problem can be reduced somewhat by assuming that the $X_i(t)$ trace is responsible for CR topography and that a different trace, $\overline{x}_i(t)$, is responsible for ISI phenomena. However, the problem remains that a stimulus trace of fixed time course cannot adequately account for the timing properties observed in CRs. Thus, what is needed, and what is lacking in $X_i(t)$, is a stimulus trace that is capable of adapting to the temporal configuration of the stimuli.

The sections that follow address these issues. Section 2 offers an alternative to the single-unit approach to modeling conditioning by presenting a network model that is ca-

[7] Inhibition of delay is a good example of how temporal expectations result in adaptive behavior. From the point of view of a biological system, a delayed response is an efficient use of resources when the US occurrence is delayed.

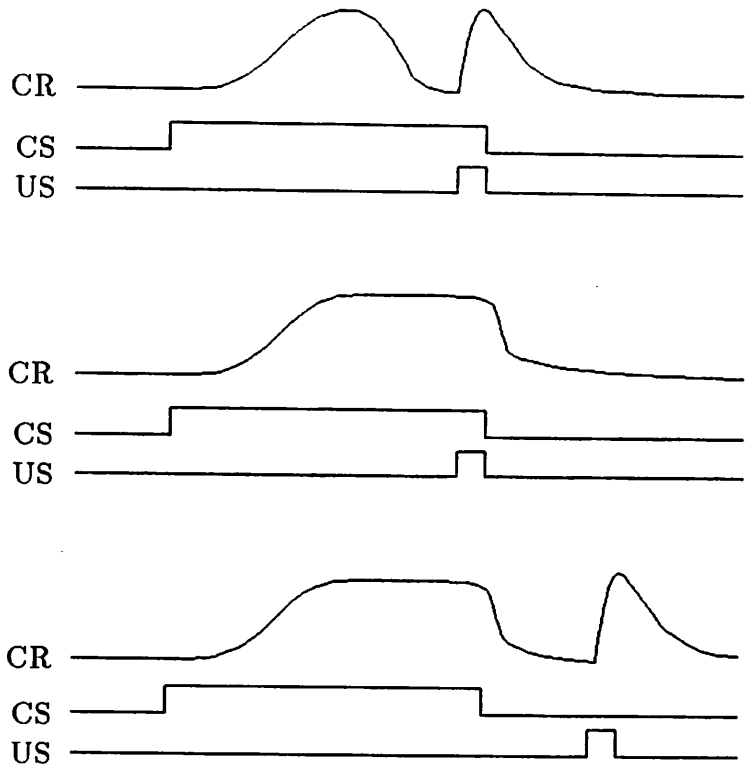


**Figure 4:** Unsuccessful CR predictions of the single-unit model. In each case, the ISI is greater than the optimal ISI. Details are described in the text.

pable of generating realistic CR waveforms. The network uses an LMS rule but avoids the problems of continual weight update by learning when update is appropriate. Whereas Section 2 concentrates on the CR-generating properties of the stimulus trace and postpones treatment of the ISI function, Section 3 addresses the question of whether the trace architecture of Section 2 can be extended to account for both properties of the stimulus trace.

## 2. A network approach

Although modeling conditioning using a single adaptive processing unit has been of limited success, the limitations of this approach have proven instructive for subsequent model development. A network model (Desmond et al., 1986; Desmond and Moore, 1988) that overcomes many of the limitations of the single-unit approach and provides a wider range of verifiable predictions (at the cost of greater complexity) is presented below. Two major changes from the one-unit approach to the network approach can be described as follows:

- The temporal properties of the stimulus trace and the CR are not represented by a single element, but are instead distributed over many elements.
- The stimulus trace serves as a clock that allows the network to learn, over repeated CS–US presentations, when the US will occur. Changes in weights that generate the CR occur only at the times when the US is "expected."

### 2.1 A multiple-element stimulus trace

The stimulus trace proposed for the network model has two basic underlying assumptions. The first assumption, which is one of function, is that the trace process is a timing mechanism initiated by changes in CS activation.[8] The second assumption of the stimulus trace regards its structure. It is assumed that the trace consists of many elements, and that the architectural arrangement of the elements mediates the timing function by transforming the temporal representation into a spatial representation. Specifically, elements are organized in what is referred to as a tapped delay-line or transversal filter, as illustrated in Figure 5. Once initiated, activation propagates along the delay line. Timing information contained in the taps can be sent to higher-order units for further processing.

For each CS, onset and offset of the stimulus activate separate tapped delay-lines. Consequently, each stimulus trace element is uniquely referenced by three indices: (a) The CS which activates it: Let $i$ refer to the $i^{\text{th}}$ CS, where $i = 1, \ldots, n$. (b) Whether its activation is linked to CS onset or CS offset: Let $j$ denote whether the element is an onset ($j = 1$) or offset ($j = 0$) element. (c) A unique element number within the delay

[8] Such changes in CS activation play an important role in Klopf's drive-reinforcement neuronal model (Klopf, 1986; 1988). However, in contrast to Klopf's model, negative changes in CS activation (i.e., CS offset) can also play a role in generating CRs.

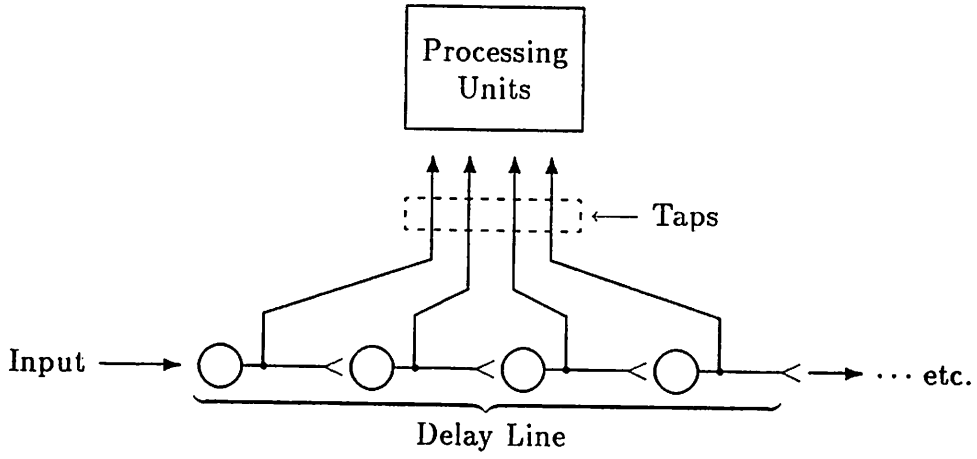


**Figure 5:** Basic tapped delay line. Injection of CS input begins sequential propagation of signal through a delay-line. Each synapse ( -< ) introduces a delay; the total delay from activation of the first element in the delay-line to the last element is a direct function of the number of sequential synapses. Taps from the delay-line units send timing information to higher-order processing units.

line: Let $k$ denote the $k^{\text{th}}$ element in the array of elements, where $k = 1, \ldots, N$. The $k$ index corresponds to the element's order of activation, where $k = 1$ corresponds to the first element in the delay-line and $k = N$ refers to the last element. The stimulus trace elements are referred to as $x_{ijk}$, and the total number of these elements is equal to $n{\times}2{\times}N$.

Thus, in the network model a *trace process* refers to the initiation and sequential propagation of activity along the elements in a tapped delay-line. At any given time step, each $x_{ijk}$ element is either in an active state $[x_{ijk}(t) = 1]$ or an inactive state $[x_{ijk}(t) = 0]$. Once activated, an element remains at 1 for an arbitrary number of time steps (10 steps in the simulations below) and then returns to 0. Thus, activity of the elements overlaps. The formal expression for the activation of an element is:

$$x_{ijk}(t) = \begin{cases} 1 & \text{if } \tau_{ij} + k - 1 \leq t < \tau_{ij} + k + 9; \\ 0 & \text{otherwise,} \end{cases} \tag{4}$$

where $\tau_{ij}$ is the onset time ($j = 1$) or offset time ($j = 0$) of CS $i$ ($x_{ijk} = 0$ if CS $i$ is not presented).

Figure 6 illustrates the basic connections within the network. The stimulus trace ($x_{ijk}$) elements make modifiable "synaptic" contacts with two computational units, V and E. These synapses are designated $V_{ijk}$ and $E_{ijk}$, respectively. Note that to simplify the figure,

only one set of $x_{ijk}$ elements are depicted as contacting the V and E units. To fully represent the network for simulating two CSs, four such sets of $x_{ijk}$ would have to be depicted, one set for the onset and offset of each CS. Thus, if the elements in the figure represent the onset trace for CS1, then using the notation described above they would be designated $x_{111}, \ldots, x_{119}$.

The V unit and the E unit both receive input from the US, designated $L(t)$, and the V unit also receives the output of the E unit, designated $r(t)$. These connections are not modifiable, as indicated by the open ( -< ) synaptic terminals in Figure 6; modifiable $V_{ijk}$ and $E_{ijk}$ connections are indicated by the closed ( -◁ ) synaptic terminals. The output of the network, $s(t)$, is derived from the US input and from the weighted sum of the V unit inputs, and is defined as:

$$s(t) = \sum_i \sum_j \sum_k V_{ijk}(t) x_{ijk}(t) + L(t), \tag{5}$$

where $s(t)$ is confined to the closed unit interval. Changes in the $V_{ijk}$ weights are given by the following expression:

$$\Delta V_{ijk}(t) = c\{L(t) - \hat{s}(t)\} h_{ijk}(t) \bar{x}_{ij}(t) r(t). \tag{6}$$

Progressing from left to right in Equation 6 are the following terms.

$\Delta V_{ijk}(t)$ denotes the change in $V_{ijk}$ from the previous time step, i.e., the difference, $V_{ijk}(t) - V_{ijk}(t-1)$.

$c$ is a constant that affects the rate of learning, $0 < c \leq 1$.

$L(t)$ is the input from the US. $L(t) = 0$ when the US is off and $L(t) = \lambda$ when the US is on, where $\lambda$ is a constant that denotes the strength of the US, $0 \leq \lambda \leq 1$. In the simulations presented below, $\lambda = 1$.

$\hat{s}(t) = \sum \sum \sum V_{ijk}(t) x_{ijk}(t)$, where $0 \leq \hat{s}(t) \leq 1$. Thus, $\hat{s}(t)$ is equal to $s(t)$ without the contribution of the US.

$h_{ijk}(t)$ is a *synaptic eligibility* for each $V_{ijk}$ synapse, where $0 \leq h_{ijk}(t) \leq 1$. When an $x_{ijk}$ element is initially activated and changes from 0 to 1, $h_{ijk}(t) = 1$ and the synapse is most eligible for modification. As time progresses the value of $h_{ijk}(t)$ decreases

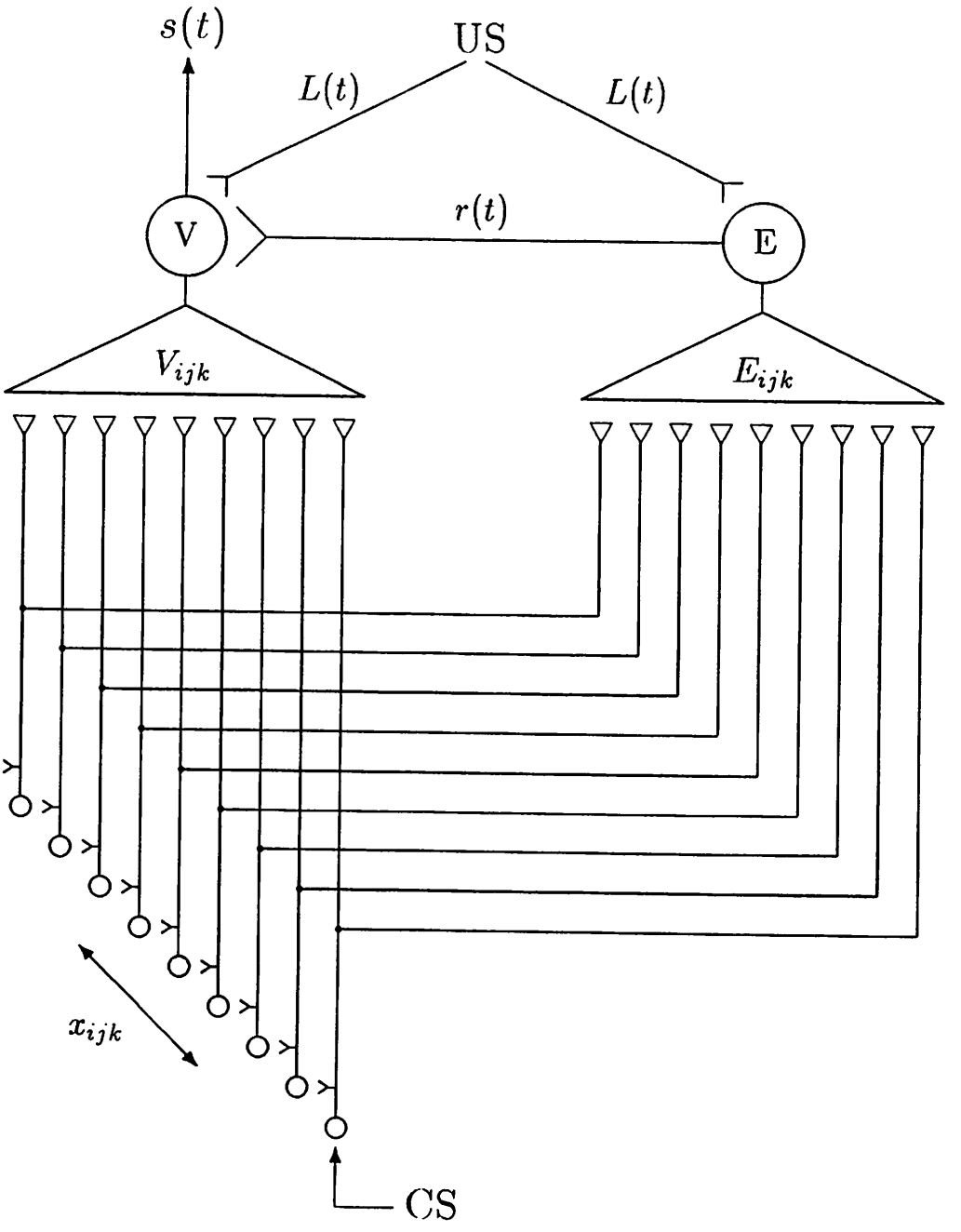


**Figure 6:** Basic organization of the network model. Stimulus trace elements are designated $x_{ijk}$. For simplicity, only 9 onset elements for a single CS (i.e., $x_{111}, \ldots, x_{119}$) are depicted; the 9 offset elements ($x_{101}, \ldots, x_{109}$) are not shown. Further details are in text. Copyright 1988, Springer-Verlag.

geometrically.[9]

$\bar{x}_{ij}(t)$ governs the rate of conditioning at a given interstimulus interval. In Section 1, the $\bar{x}_i(t)$ eligibility trace term was described as a function that governs the rate of change in synaptic weight. Because activation of the CS implied activation of the synapse in the single-unit model, no distinction was made between synaptic and CS–US eligibility. However, with the multi-synaptic representation of the network, CS activation is no longer synonymous with synaptic activation, so two distinct eligibilities exist. For the present, the reader can consider this term as a "built-in" inverted-U shaped function that mimics the empirically observed interstimulus interval function but does not explain it.[10] This term is discussed in more detail in the next section, where it is argued that by modifying the tapped delay-line architecture, the $\bar{x}_{ij}(t)$ term can be eliminated.

$r(t)$ is the output of the E unit, and represents the "temporal expectation" of reinforcement, $0 \leq r(t) \leq 1$. $r(t)$ is defined as:

$$r(t) = \max\{E_{ijk}(t)\Delta x_{ijk}(t) \mid i = 1,\ldots,n;\ j = 0,1;\ k = 1,\ldots,N\} \tag{7}$$

where:

$$\Delta x_{ijk}(t) = \begin{cases} 1 & \text{if } x_{ijk}(t) - x_{ijk}(t-1) = 1; \\ 0 & \text{otherwise,} \end{cases} \tag{8}$$

and $E_{ijk}$ are the connection weights of the input elements onto the E unit. Changes in these weights are given by:

$$\Delta E_{ijk}(t) = c[L(t) - r(t)]\Delta x_{ijk}(t)\bar{x}_{ij}(t) \tag{9}$$

where $\Delta x_{ijk}(t)$ is defined as in Equation (8).

---

[9]The synaptic eligibility, $h_{ijk}(t)$ was computed as follows:

$$h_{ijk}(t) = \begin{cases} 1.0 & \text{if } t = \tau_{ij} + k - 1; \\ (0.8)h_{ijk}(t-1) & \text{if } t > \tau_{ij} + k - 1; \\ 0.0 & \text{otherwise,} \end{cases}$$

[10]The actual equations are:

$$\bar{x}_{ij}(t) = \begin{cases} (.05)(t - \tau_{ij}) - 0.25 & \text{if } \tau_{ij} + 6 < t < \tau_{ij} + 25; \\ (-1/475)(t - \tau_{ij}) + (500/475) & \text{if } \tau_{ij} + 25 \leq t < \tau_{ij} + 500; \\ 0.0 & \text{otherwise.} \end{cases}$$

Equation (6) states that in order for a $V_{ijk}$ synapse to change weight there must be a discrepancy between the actual reinforcement and the output "predicted" by the V unit, i.e., $L(t) - \hat{s}(t) \neq 0$. The other three variables, $h_{ijk}(t)$, $\overline{x}_{ij}$, and $r(t)$ collectively determine the rate of change in the synaptic weight. Note that from Equation (9), an $E_{ijk}$ synapse is eligible to change weight only when its corresponding $x_{ijk}$ element is initially activated (i.e., $\Delta x_{ijk}(t) = 1$). Thus, in contrast to $V_{ijk}$ synapses, which remain eligible for several time steps after initial activation, $E_{ijk}$ synapses are eligible for only one time step. Consequently, $E_{ijk}$ weights can change only if the synapse is activated during US presentation.

Equations (7) and (8) indicate that an $E_{ijk}$ weight contributes to the output signal $r(t)$ only when the corresponding $x_{ijk}$ element is initially activated. The net effect of Equations (7), (8), and (9) is that the E unit provides discrete bursts of activity to the V unit at times of US expectation, i.e., the bursts occur at temporal loci where previous presentations of the US have occurred. It is only when these expectation signals occur that $V_{ijk}$ synapses are allowed to change.

## 2.2 Basic network dynamics

The dynamics of the network on the second trial of acquisition training are illustrated pictorially in Figure 7. Although the delay-line portion of the stimulus trace is omitted from view and only the taps are depicted, the connectivity in this figure is identical to that depicted in Figure 6. Each panel of Figure 7 represents the state of the network at four different time steps. The upper right corner of each panel shows the current time step and the temporal configuration of the stimuli. The activation levels of $x_{ijk}(t)$, $L(t)$, and $r(t)$ are denoted by the "axons" carrying those signals. A solid-line axon means that the term is equal to zero. A dashed-line axon for $x_{ijk}(t)$ or $L(t)$ means that the term is equal to one; for $r(t)$ it means that $r(t) > 0$. (A weak $r(t)$ signal is depicted as a single dashed line, whereas a strong $r(t)$ signal is shown as two parallel dashed lines.) Circles are used to depict relative magnitudes of other terms in the model (magnitude proportional to diameter) and whether those terms are positive (open-circles) or negative (filled-circles). The magnitudes of $s(t)$ and $\hat{s}(t)$ are represented by the lengths of the vectors emanating from the top of the V unit.

The first thing to note in Figure 7 is the sequential and overlapping activation of the $x_{ijk}$ elements for $t = 1$ to $t = 4$. The circles directly above the $x_{ijk}$ terminals represent the degree of synaptic eligibility ($h_{ijk}$ for the $V_{ijk}$ weights and $\Delta x_{ijk}$ for the $E_{ijk}$ weights). For simplicity, the $x_{ij}(t)$ term is not represented in the figure and is assumed to be equal to 1 at all time steps.

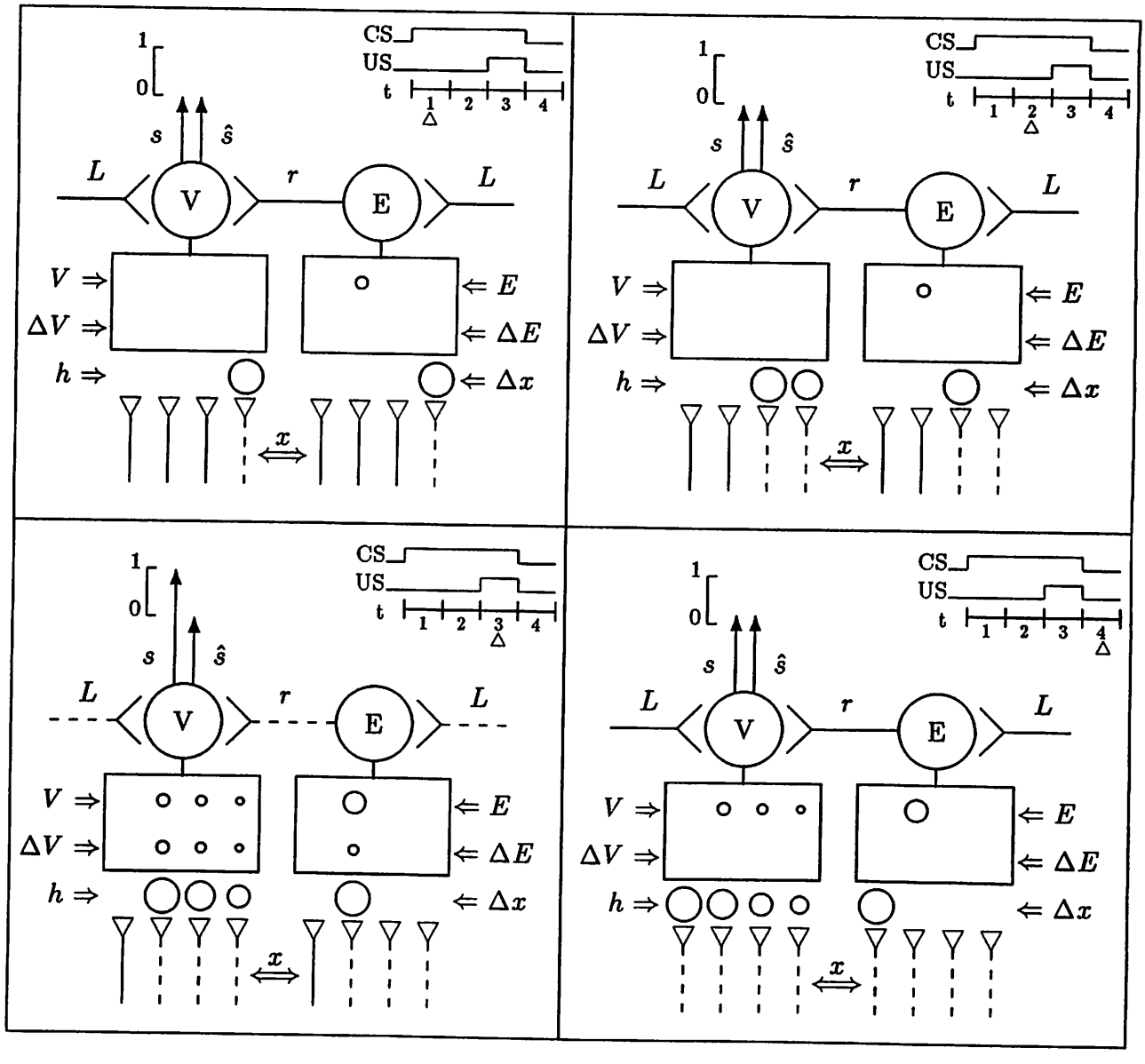


**Figure 7:** Network dynamics during early acquisition training. See text for details.

The $V_{ijk}$ and $E_{ijk}$ weights, along with the changes in these weights ($\Delta V_{ijk}$ and $\Delta E_{ijk}$) are also depicted in Figure 7. Note that one of the $E_{ijk}$ weights has a small positive initial value; this value was obtained on the first training trial. None of the $V_{ijk}$ weights changed on trial one because such changes require a positive $r(t)$ signal, which in turn requires some existing $E_{ijk}$ weight. Thus, trial 2 is depicted in Figure 7 so that the reader can observe changes in both $V_{ijk}$ and $E_{ijk}$ weights. As illustrated in the lower left panel of the figure, these changes occur at time step $t = 3$. It is evident that more recently activated synapses gain greater amounts of associative strength than less recently activated synapses.

Figure 8 illustrates network dynamics during extinction training. Note that three $V_{ijk}$ weights and one $E_{ijk}$ weight start out at asymptotic levels and are represented in the figure by relatively large circles. At time $t = 3$, the E unit sends a strong $r(t)$ signal to the V unit, allowing changes in $V_{ijk}$ weights to occur. Because $L(t)$ is 0 (due to the absence of the US) and $\hat{s}(t)$ is approximately equal to 1 in Equation (6), changes in $V_{ijk}$ are negative, as depicted by the filled circles. A negative change in synaptic weight similarly occurs for the $E_{ijk}$ synapse by Equation (9).

In the preceding examples of acquisition and extinction, only 4 $x_{ijk}$ elements were used to generate CRs. For more realistic simulations of CR waveforms more elements are required. In the simulations presented below, each stimulus trace is comprised of at least 50 elements.

## 2.3 Network simulations of conditioning paradigms

**Delay conditioning.** Figure 9 illustrates simulated response topographies for early, middle, and late stages of acquisition and extinction training in a delay conditioning paradigm.[11] During early stages of acquisition the CRs tend to occur just prior to US onset, and from the simplified example in Figure 7 it should be clear why this occurs: $V_{ijk}$ synapses gain considerably more strength when activated concurrently with reinforcement than they do when synaptic eligibility is allowed to decay. Thus, in early acquisition training, only those elements that are activated at or just prior to US onset will possess enough weight to drive the output above threshold level. As acquisition proceeds, elements that are activated at earlier times relative to US onset become capable of generating detectable output. This point is illustrated in Figure 10, which is a learning curve over acquisition

[11] In order to simulate physiological threshold and recruitment effects at motoneurons controlling the CR, a smoothed and thresholded function of $s(t)$, designated $Y(t)$, is presented in Figure 9 and in subsequent figures. $Y(t)$ is defined as $\sum_{i=0}^{i=2}|.8s(t-i) + .2Y(t-i-1)|/3$, if $Y(t) > 0.1$; otherwise $Y(t) = 0.1$.

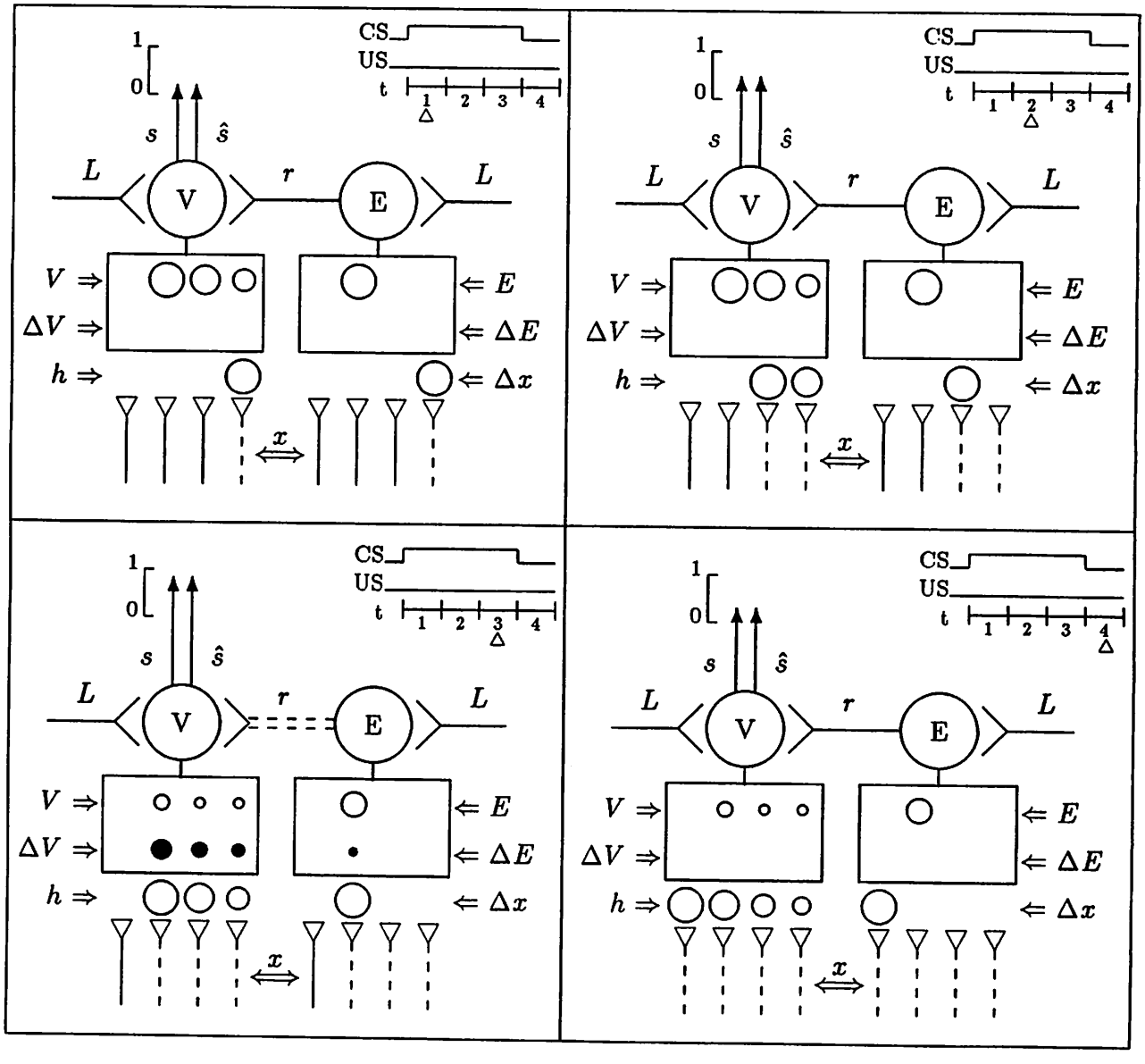


**Figure 8:** Network dynamics during early extinction training. See text for details.

and extinction training for all the onset elements. Also evident in the acquisition phase of Figure 10 is that associative strength increases over training as an S-shaped function.

Figure 11 illustrates the $V_{ijk}$ weights for the onset and offset elements at asymptotic acquisition training. The weights, which are depicted as solid bars, are represented at their times of initial activation (i.e., each $V_{ijk}$ is depicted at the time step when the corresponding $x_{ijk}$ element changes state from 0 to 1). Note that the depiction of onset weights in Figure 11 is essentially a "slice" from Figure 10; the slice is cut perpendicular to the Trials axis where the acquisition phase ends, and is parallel to the $k$ axis. The weights for the offset elements are zero because these elements have $h_{ijk} = 0$ at US onset. Thus, in this simulation the CR is generated solely by the weights of the onset elements.

**Trace conditioning and a novel prediction.** In contrast to the results from delay conditioning, offset weights can gain considerable strength in a trace conditioning protocol, as illustrated in the upper left panel of Figure 12. The CR depicted in the lower left panel of the figure is generated by the summation of the onset and offset weights [Equation (5)]. However, because the onset and offset trace processes are assumed to be independent, the model predicts that the temporal overlap of these weights can be prevented by manipulating CS duration. Such a procedure is shown on the right side of Figure 12. The prediction of the network is that after trace conditioning training trials, if a CS of extended duration is administered as a probe trial, the onset and offset weights become temporally displaced as illustrated in the upper right panel, and a bimodal CR is generated (lower right panel). Furthermore, each peak of the bimodal CR is half the amplitude of the composite unimodal CR.

**Changing US timing.** The simulation in Figure 13 demonstrates the *micromolar* nature of this network. In micromolar constructs of conditioning (Logan, 1956), CRs of different latencies are considered to be *different responses.* In the network model, they truly are different responses because they are generated by different elements. Thus, a CR that develops at a short interstimulus interval, as illustrated in the top panel of Figure 13, extinguishes when the interstimulus interval is lengthened. A different CR then develops independently at the new US locus. The middle and bottom panels of the figure show the gradual extinction of the short-latency CR and the establishment of the longer-latency CR, a result consistent with experimental findings (Boneau, 1958; Gormezano and Moore, 1969; Leonard and Theios, 1967).

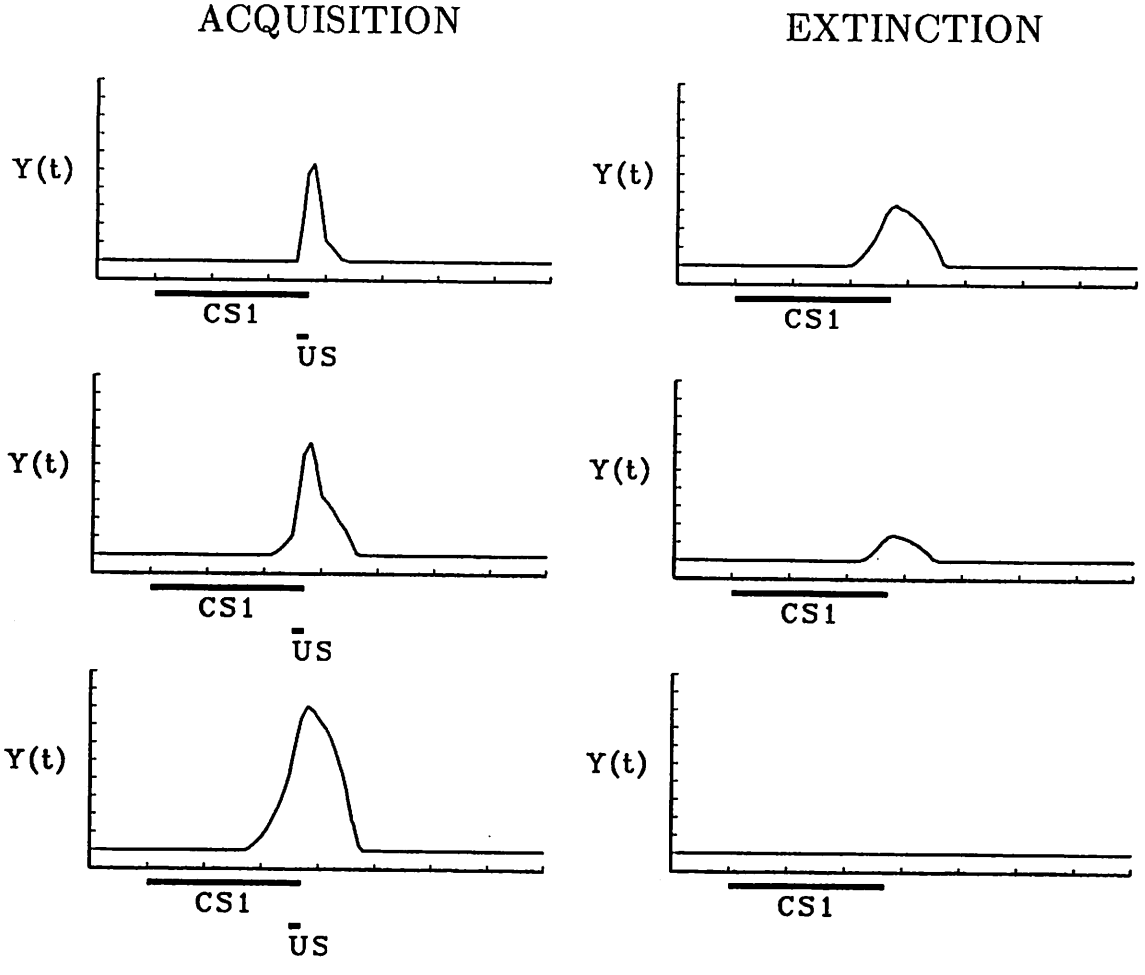


**Figure 9:** Simulated conditioned response topographies for aquisition and extinction training in a delay conditioning paradigm. Hash marks on X-axis denote 10 time steps. Simulation parameters: $c = 0.05$, number of $x$ elements = 100 total, time steps/trial = 80. Early, middle, and late CR waveforms obtained at 5, 10, and 25 trials of training, respectively. Copyright 1988, Springer–Verlag.

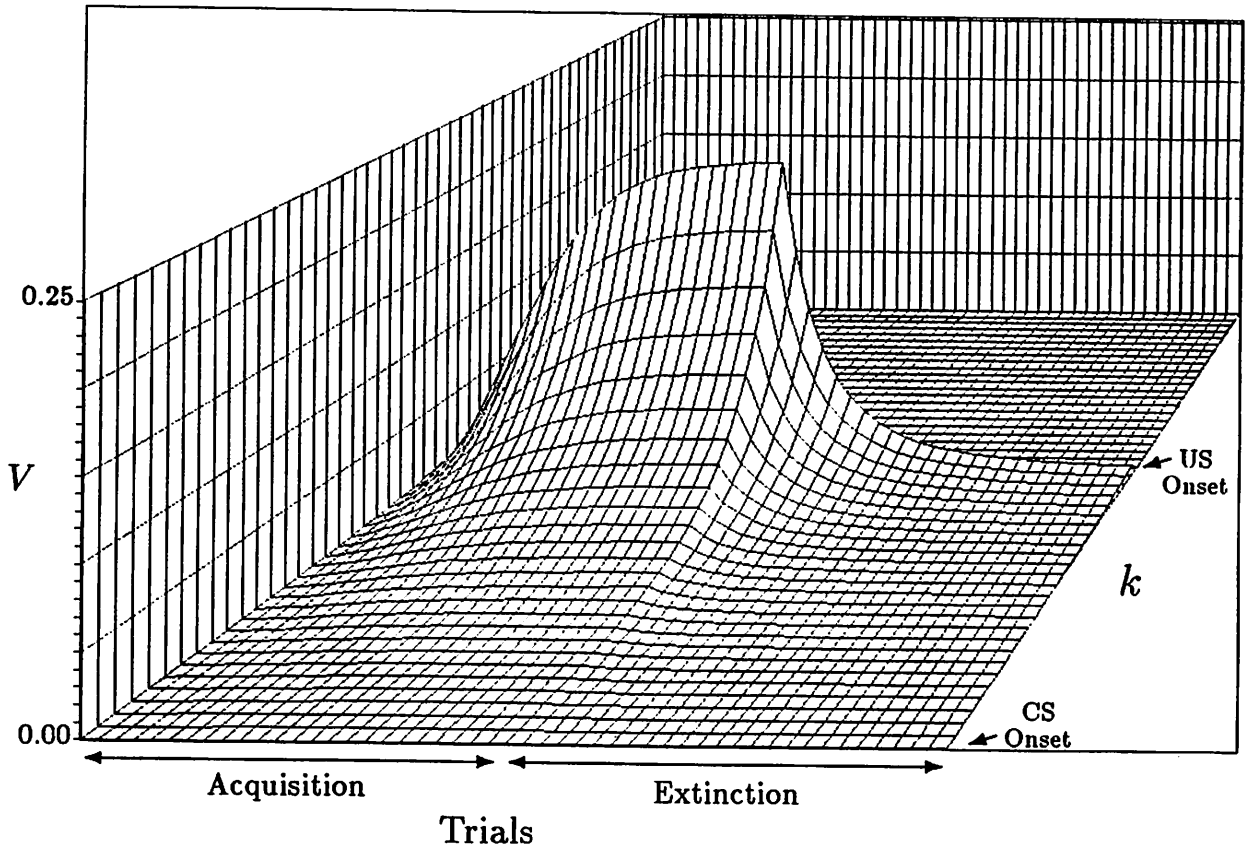


**Figure 10:** Synaptic weight ($V$ axis) over acquisition and extinction trials (horizontal axis) for each of the $k = 1, \ldots, N$ onset elements (remaining axis, k=1 is closest to reader). Copyright 1988, Springer–Verlag.

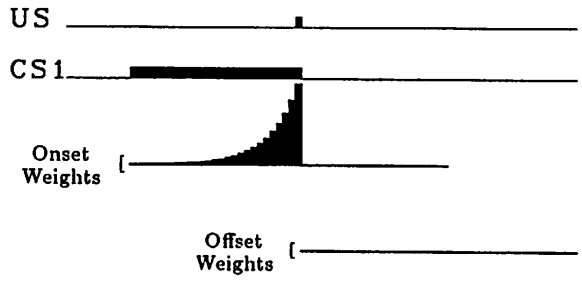


**Figure 11:** The $V_{ijk}$ weights at asymptotic acquisition for delay conditioning. Weights are depicted as solid vertical bars, and the magnitude of each weight is represented by the height of the bar. Time progresses from left to right, and each weight is depicted at the time in which its corresponding $x_{ijk}$ element is initially activated. Bars extending above the horizontal line represent positive weights. Bars that extend below the horizontal line are negative. Simulation parameters are those listed for Figure 9.

**Blocking.** The network model is capable of simulating the results of Kamin's blocking paradigm (Kamin, 1968). A blocking simulation is illustrated in Figure 14. This paradigm is conducted in three stages. In the first stage (top panel), CS1–US trials are presented until asymptotic CRs are generated. In the second stage (middle panel) a different CS (CS2) is presented in compound with CS1, and the compound is paired with the US. An equal number of trials are presented in stages 1 and 2 of the simulation. In stage 3, the ability of CS2 to generate CRs is tested. In agreement with experimental results (e.g., Marchant and Moore, 1973), CS2 does not elicit a CR. The $V_{ijk}$ for CS2 (i.e., the $V_{2jk}$) do not gain strength for the same reason that $V$ does not increase in the Rescorla-Wagner (1972) model—the discrepancy between the reinforcement and the prediction is close to zero, i.e., $L(t) - \hat{s}(t) \approx 0$ in Equation (6), due to the large positive weights of CS1.

**Conditioned inhibition.** Simulation results for conditioned inhibition are illustrated in Figure 15. In this paradigm two trial types are alternately presented.[12] For the first type, designated (CS1)+, CS1 is paired with the US, and for the second type, designated

[12]In behavioral experiments the two trial types are typically presented in a random or pseudorandom sequence. In simulations, the two types are simply alternately presented. Given a large enough number of trials and equally probable trial types, the simulation results would be identical for random and alternating sequences.

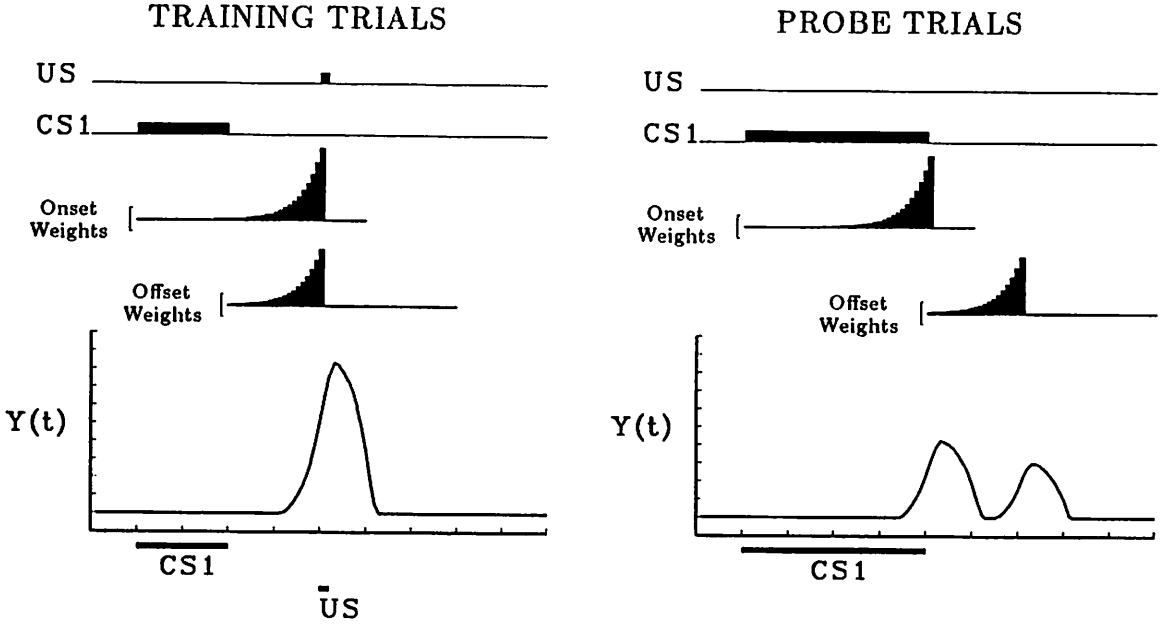


**Figure 12:** The temporal distribution of onset and offset weights in trace conditioning, and a prediction of CR topography when the timing of onset and offset processes is shifted. **Left:** When a trace conditioning protocol is simulated, both onset and offset weights develop excitatory strength. The unimodal CR that results is generated by the summation of the two sets of weights. **Right:** If, after trace conditioning training, the duration of the CS is extended, the onset and offset weights contribute to the CR at different times and a bimodal CR is predicted. Simulation parameters: $c = 0.2$, number of $x$ elements = 100 total, time steps/trial = 100. Bottom left CR was obtained after 15 training trials. Bottom right CR was obtained on first subsequent probe trial. Modified from Desmond and Moore (1988).

(CS1/CS2)–, a CS1/CS2 compound is not paired with the US. The left portion of Figure 15 depicts the two trial types and the predicted CRs at the end of the simulation run (after weights have reached asymptotic levels). The right side of the figure depicts the asymptotic weights for CS1 and CS2. Note that the weights for CS2 are negative (bars extend below the horizontal line).

**Manipulations of inhibitory weights: Millenson et al. simulation.** Under the network representation of conditioned inhibition, CRs are cancelled out on CS1/CS2 compound trials because positive and negative weights contribute to the system's output *at the same time.* By selecting appropriate training and testing procedures, the timing of the

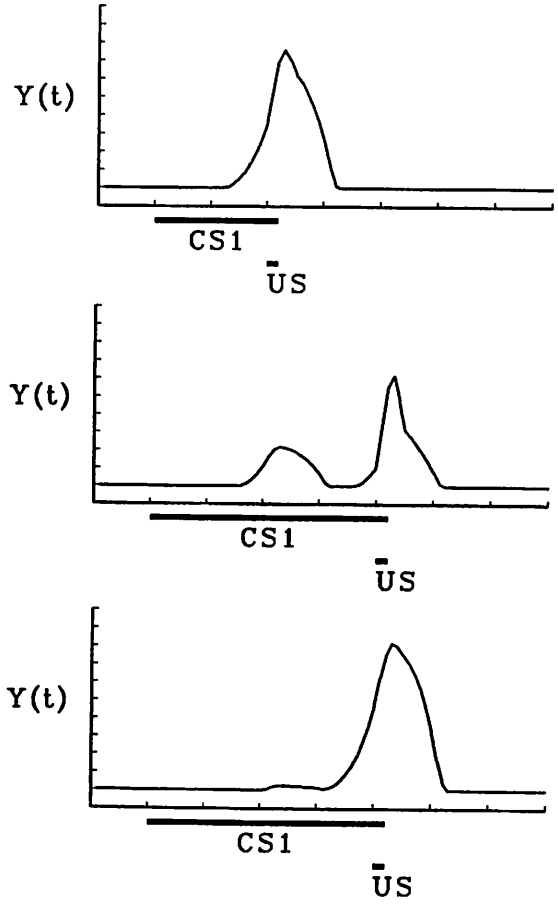


**Figure 13:** Effects of changing US timing on CR topography. **Top:** In Stage 1, 25 short CS–US interval training trials are presented. **Middle:** In Stage 2, the CS–US interval is lengthened. After 10 trials, the short-latency CR is somewhat diminished and a longer-latency CR begins to develop. **Bottom:** After 30 Stage 2 trials, transformation of CR topography is nearly complete. Simulation parameters for both stages: $c = 0.05$, number of $x$ elements = 120 total, steps/trial = 80.

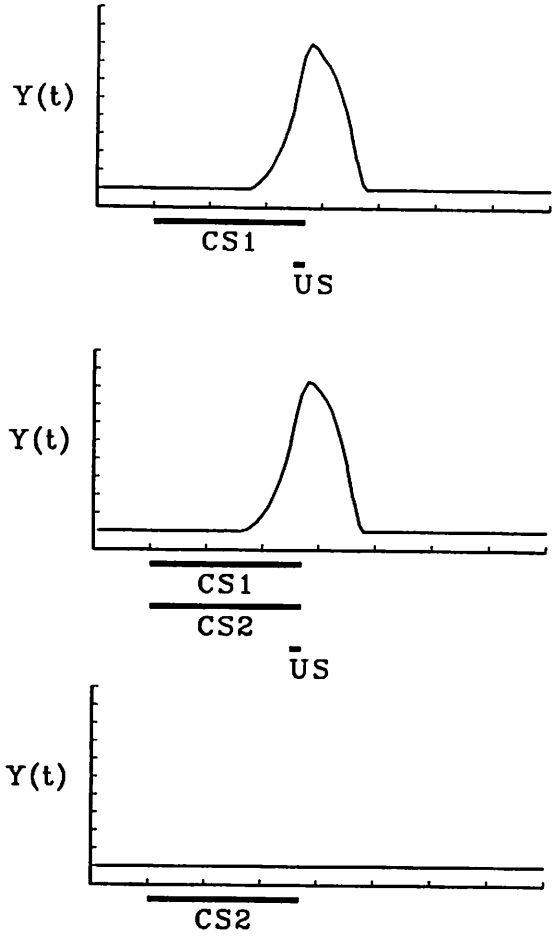


**Figure 14:** Simulation of Kamin's blocking paradigm (Kamin, 1968). See text for details. Simulation parameters: $c = 0.05$, number of $x$ elements = 100 total, time steps/trial = 80. Stage 1 (top) and Stage 2 (middle) CR profiles are after 25 training trials. Stage 3 testing (bottom) consists of 1 trial.

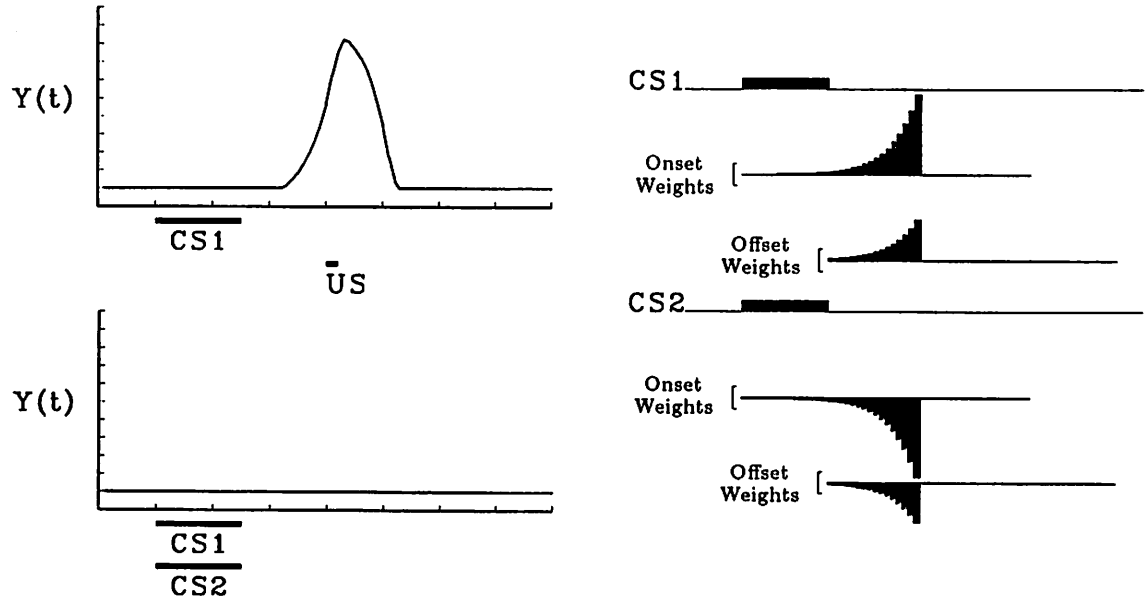


**Figure 15:** Simulation results for conditioned inhibition. CR profiles after 30 trials for (CS1)+ and (CS1/CS2)- trial types are depicted in the upper and lower left panels, respectively. The temporal distribution of the $V_{ijk}$ weights on a (CS1/CS2)- trial is depicted on the right side of the figure. Simulation parameters: $c = 0.15$, number of $x$ elements = 200 total, time steps/trial = 80.

inhibitory weights can be manipulated to either cancel or fail to cancel the effects of positive weights. This property of the model is demonstrated by simulating one experimental group from a study by Millenson, Kehoe, and Gormezano (1977). In this experiment, rabbits were trained to give conditioned nictitating membrane responses to a single tone CS in a delay conditioning paradigm; however, unlike simple acquisition training, the CS–US interval was not constant over trials, and could take on either short (200 ms) or long (700 ms) values. The proportion of the short and long trial types was varied across 5 groups, with the proportion ranging from 0 to 1. The simulated group was the one designated P 1/2 by Millenson et al. (1977) to denote a 50:50 mixture of short and long trial types.

Simulation results for the P 1/2 group are presented in Figure 16. CRs generated on short and long CS-alone probe trials are shown. The figure reveals that on short CS probe trials, the CR waveform is essentially unimodal, whereas a bimodal CR is generated on long CS probe trials.

Figure 17 illustrates how these CRs are generated by displaying the temporal configu-

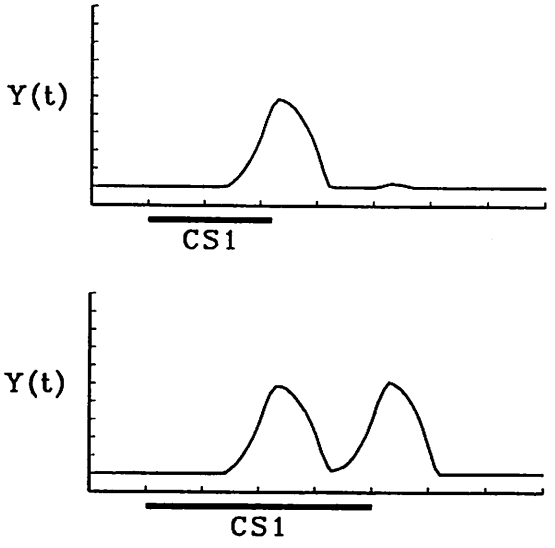


**Figure 16:** Simulation results for group P 1/2 of the Millenson et al. (1977) study. CR topographies for short CS (top panel) and long CS (bottom) CS-alone test trials are depicted. Copyright 1988, Springer–Verlag.

ration of the positive and negative weights on both trial types. Note that because the US occurs at two different interstimulus intervals, two loci of US expectation develop (i.e., for each trial, $r(t) > 0$ at two different times) and two sets of positive onset weights develop around these US expectations. Initially, these weights tend to generate bimodal CRs on both trial types. However on short trial types, the following events occur: (a) the CS terminates at the first point of US expectation; (b) the offset of the CS intiates the offset trace; (c) at the second point of US expectation, $r(t) > 0$ while the offset elements are active; (d) the US does not occur, i.e., $L(t) = 0$; and (e) CR output is generated around the second US expectation, i.e., $\hat{s}(t) > 0$. By Equation (6), the latter conditions lead to negative changes in $\Delta V_{ijk}(t)$ for the offset elements. Over a number of presentations of the two trial types, negative offset weights continue to develop until they ultimately cancel the positive onset weights on short CS trials. On long CS trials, the offset process is initiated after the excitatory weights have contributed to the CR and thus, the negative weights do not cancel the second CR peak.

The experimental results for Millenson et al. (1977) are shown in Figure 18, which depicts averaged conditioned nictitating membrane extension as a function of time on acquisition days 3 and 10 for short (left column) and long (right column) CS-alone probe

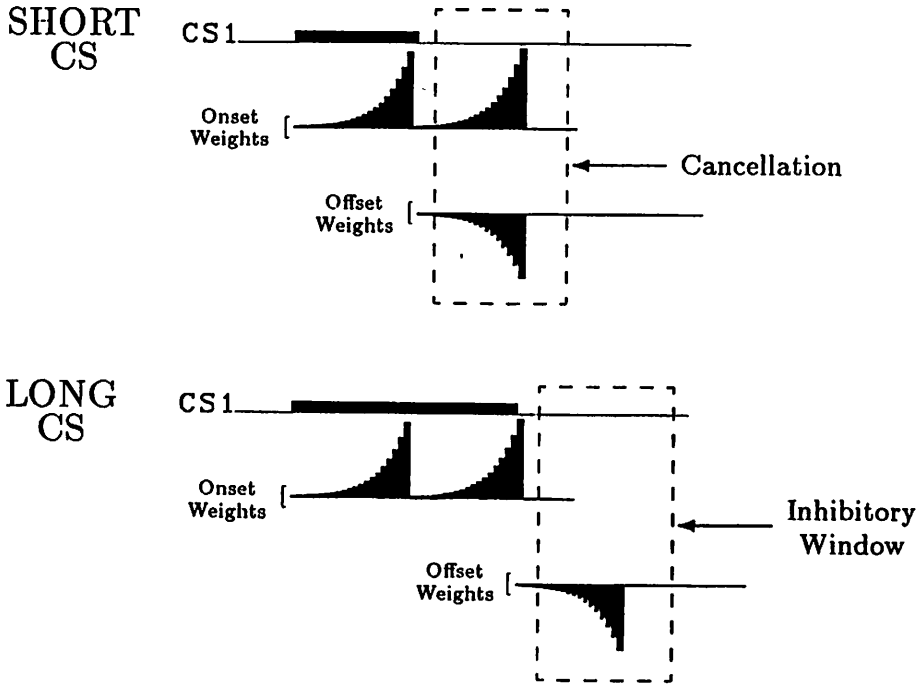


**Figure 17:** The $V_{ijk}$ for the simulation of Millenson et al. (1977), represented at their times of activation on short CS and long CS trials. Cancellation of excitatory onset weights and inhibitory offset weights results in a unimodal CR on short CS test trials. The non-cancellation on long CS test trials results in a bimodal CR and a period of inhibition after CS offset. Copyright 1988, Springer–Verlag.

trials. The results for the P 1/2 group are found in the middle row of this figure. The reader will notice that the experimental and the simulated CR waveforms are similar in that CRs on short CS trials are basically unimodal, but are bimodal on long CS trials; in addition, each CR peaks at a time of US onset. Also note that the CR to the short CS displays a slight tendency for a second peak. In the network, this minute second peak is attributed to an incomplete development of inhibitory weights in the offset elements. The simulated CR to the short CS in Figure 16 exhibits a small second peak due to incomplete cancellation of excitatory and inhibitory weights. With extended training inhibitory weights completely cancel excitatory weights.

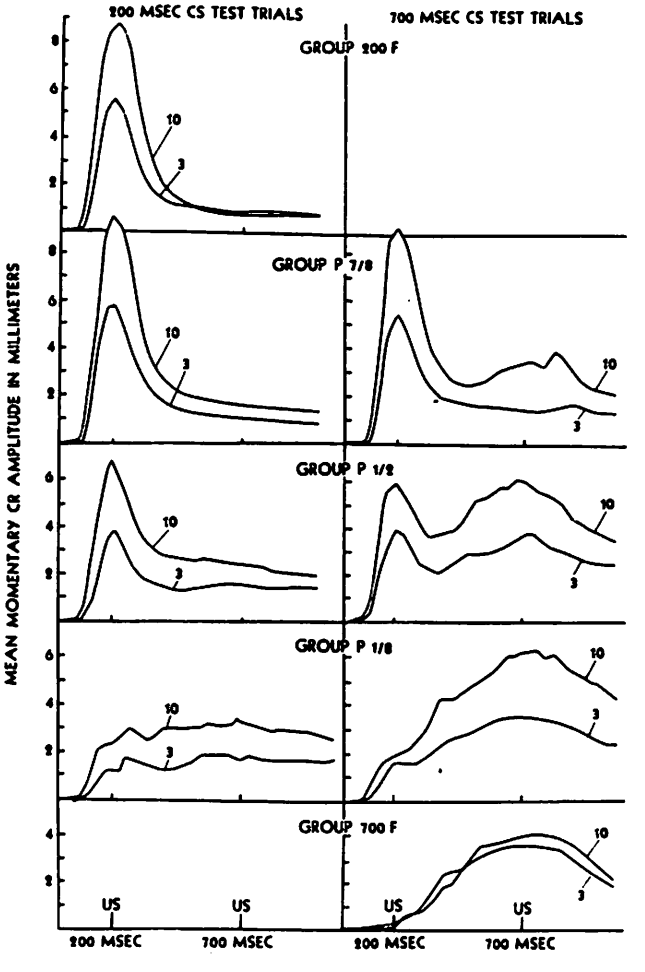


**Figure 18:** Experimental results of Millenson et al. (1977) study. The waveforms represent group mean nictitating membrane movement on acquisition days 3 and 10 for short (left side) and long (right side) CS test trials. Copyright 1977 by Academic Press. Reproduced by permission.

**A corollary prediction.** If the experimental outcome of Millenson et al. (1977) is indeed a result of the temporal arrangement of excitatory and inhibitory weights, as predicted by the network and as illustrated in Figure 17, then an additional prediction of the network can be tested experimentally. This prediction is illustrated in the lower panel of Figure 17, where it can be seen that on long CS trials, an inhibitory temporal window is generated by the negative weights of the offset elements. Thus, the network predicts that this temporal window should exhibit behaviorally testable properties of a conditioned inhibitor. Specifically, the window can be tested with standard tests for inhibition (e.g., Marchant, Mis, and Moore, 1972; Rescorla, 1969).

1. *Summation test.* Suppose that, in addition to training subjects on the Millenson et al. (1977) P 1/2 protocol using a tone CS, subjects are also trained to give CRs to a second CS (e.g., a light). Once the Millenson et al. effect is observed to the tone CS, probe trials consisting of long tone followed by light are presented. The network predicts that the light CR should be inhibited if it occurs after long tone offset, due to the summation of excitatory (light CS) weights and inhibitory (tone offset) weights.

2. *Retardation test.* The logic of this test is as follows. If the offset of the long tone results in a temporal window of inhibition, then it should be relatively difficult to establish CRs in this window because existing inhibition would have to be overcome first. Thus, retardation testing would be conducted in two stages. Stage 1 consists of training on the P 1/2 protocol. Stage 2 consists of trace conditioning using the long tone CS, i.e., the US occurs after the offset of the long CS. The prediction of the network is that the rate of CR development within the trace interval should be slow (relative to control groups), due to the presence of negative offset weights.

# 3. Interstimulus interval effects and the stimulus trace

In the simulations presented in the previous section, ISI effects on conditioning were incorporated in the network by the function designated $\bar{x}_{ij}(t)$. This term produces ISI effects by governing the rate of change in the $V_{ijk}$ and $E_{ijk}$ synapses [Equations (6) and (9)], i.e., $\bar{x}_{ij}(t)$ exerts its effect at the level of the synapse. Theorists have speculated as to how ISI phenomena could be synaptically mediated, and some have suggested possible intracellular processes that could influence the modifiability of a synapse (Gingrich and Byrne, 1987; Sutton and Barto, 1981). Although intracellular processes such as calcium diffusion and transmitter mobilization may be important in regulating synaptic changes, synaptic regulation is not the only way to account for ISI phenomena. In fact, experimental studies have failed to demonstrate ISI effects at the single-neuron level (Kelso et al., 1986; Wigstrom et al., 1986). This section explores an alternative mechanism for explaining the ISI function, one in which the effect of ISI does not occur at the synaptic level but rather occurs at the system output level. Stimulus trace elements are given neurobiological qualities such as divergence of outputs, convergence of inputs, and sensitivity to temporal/spatial summation. When activation is allowed to propagate throughout a large collection of these elements, ISI effects emerge from the resulting patterns of spreading activation.

## 3.1 Assumptions

The ability of the tapped-delay line architecture to generate appropriate CR waveforms occurs by virtue of the forward propagation of activation of elements in the stimulus trace. In attempting to alter the architecture to include ISI effects, it is desirable to leave this basic timing mechanism intact. With this goal in mind, note two assumptions regarding the $x_{ijk}$ elements presented in Section 2: (a) Once the delay-line is activated, the number of elements recruited (i.e., changing from 0 to 1) at any given time step is always equal to one. (b) The synaptic weights of these elements on the V and E units are not bounded by any limiting value; they are determined only through the dynamics of Equation (6).

Suppose these two assumptions were changed as follows. *Change 1:* The stimulus trace is now such that the number of elements recruited at any given time is not constant, but is instead some function of time. *Change 2:* The synaptic weights of these elements are now bounded by some upper bound, $V_{\text{lim}}$.

The consequences of these changes can be seen by comparing two cases, one in which the US occurs at time $t_1$, and the other in which the US occurs at time $t_2$ ($t_1$ and $t_2$ are times

relative to the start of the stimulus trace, which in both cases occurs at $t_0$). Assume that as a result of Change 1, the number of elements recruited and thus, eligible for modification, at $t_1$ (call this number $n_1$) is greater than the number of elements recruited at $t_2$ (call this number $n_2$), i.e., $n_1 > n_2$. It follows that the CR at $t_1$ increases in magnitude faster than at $t_2$, because more synapses are modified when the US occurs at $t_1$ and therefore more elements contribute to the CR waveform. It also follows that when all the synapses that contribute to the CR at times $t_1$ and $t_2$ reach the upper weight bound $V_{\text{lim}}$, the total synaptic weight available for generating the CR at $t_1$ is greater than that at $t_2$, because $n_1 V_{\text{lim}} > n_2 V_{\text{lim}}$.

In other words, the consequences of the two proposed changes are that CRs: (a) increase in magnitude over trials at different rates depending on the ISI, and (b) reach different asymptotic magnitudes depending on the ISI. Thus, ISI effects on conditioning can be achieved given the assumed changes, but two major questions remain. The first is how a tapped delay-line stimulus trace might recruit different numbers of elements at different times? The second is, given that such a stimulus trace exists, what mechanism would allow the number of elements recruited as a function of time to resemble the empirically observed inverted-U-shaped ISI function?

In order for it to be possible to recruit different numbers of elements at different times, the one-dimensional array of elements depicted in Figure 6 is replaced by a two-dimensional planar array of elements as illustrated in Figure 19. If these elements were to be used in a full-scale network model of conditioning, they would be referred to as $x_{ijkm}$ elements,[13] where $i$ and $j$ would index, respectively, CS and onset/offset process as before, $k$ would index the column or layer that the element was in, and $m$ would index its row. However, because the $i$ and $j$ subscripts are not needed in the ensuing discussion of the trace, they are dropped and the elements are simply referred to as $x_{km}$.

It is assumed that each $x_{km}$ element not only activates the element directly in front of it—i.e., in the next column but in the same row—but also activates elements in adjacent rows. The elements thus exhibit *divergence* of outputs and *convergence* of inputs; these characteristics are evident in Figure 19, where CS input arriving on the left side of the figure is seen as initiating propagation of activation throughout the planar array.

[13] For each CS of different modality, onsets and offsets are assumed to be represented by separate planar arrays of elements, similar to the assumptions that were made for the simpler $x_{ijk}$ stimulus trace described previously. Not illustrated in Figure 19 are the connections that each element in the planar array would have with the V and E units (i.e., the taps) in a full-scale implementation of the network.

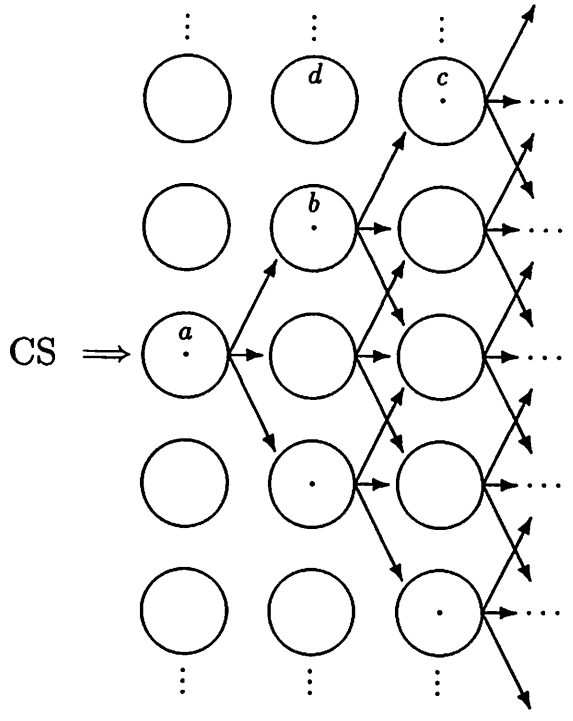


**Figure 19:** Modification of the tapped delay-line stimulus trace for a planar array of elements (taps not depicted). CS input initiates the stimulus trace by activating element *a*. Each element, in addition to activating the element directly in front of it (as in Figure 5), also activates neighboring elements in the next column. The total number of elements that a given element activates is referred to as the fan-out factor. In this figure, the fan-out factor is 3. Although all elements have the same fan-out factor, for illustration purposes only outputs of non-zero magnitude are indicated as arrows. For example, element *c* receives input from element *d*, but because the element *d*'s output activation has zero magnitude no arrows emanate from it. The only non-zero input to element *c* comes from element *b*. Elements that lie along the edges of the spreading activation are referred to as *edge elements*; in the figure these elements have dots in their centers. Non-edge elements that participate in the spreading activation (i.e., have non-zero magnitude of activation) are referred to as *interior* elements.

Figure 20 depicts an arbitrary element, $x_{km}$, from the planar array. The element is depicted as having an output occurring at time $T_{km}$ and with activation magnitude $A_{km}$. The element sends its output[14] to $N$ elements in the next column and also receives $N$ inputs from the previous column. The number $N$ is referred to as the *fan-out factor*; in Figure 19 the fan-out factor is 3. For computational simplicity, the fan-out factor can only take values such as 3, 5, 7, etc., or in general, $N = 2d + 1$, where $d$ is a positive integer. Thus, with a fan-out factor of $N$, element $x_{km}$ receives input from elements $x_{k-1\ m-d}, \ldots, x_{k-1\ m+d}$, with these inputs occurring at times $T_{k-1\ m-d}, \ldots, T_{k-1\ m+d}$ and with activation magnitudes $A_{k-1\ m-d}, \ldots, A_{k-1\ m+d}$.

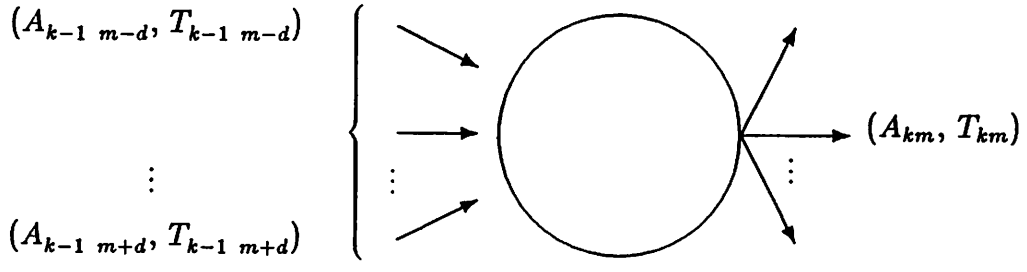


**Figure 20:** A single element, $x_{km}$, taken from the planar array of stimulus trace elements. The element receives $N$ inputs from the previous column (column $k-1$), where $N$ is the fan-out factor ($N = 2d + 1$, where $d$ is a positive integer). Each of the inputs from column $k-1$ may arrive at a different time and with a different magnitude of activation. Based upon the total contribution of its inputs, an output of activation magnitude $A_{km}$ occurring at time $T_{km}$ is sent to $N$ elements in the next layer.

Note that in contrast to the stimulus trace $x_{ijk}$ elements described in Section 2, the output activation of a planar array $x_{km}$ element, $A_{km}$, is not a binary value, but instead can range from 0 to an upper bound $\theta_{\text{up}}$. Furthermore, $x_{ijk}$ elements propagate activation from one column to the next with no loss of activation magnitude. However, for $x_{km}$ elements

[14] If one wished to conceptualize these elements as neurons, "$A$" might be analogous to the rate of firing of the neuron, and "$T$" might be the time at which a train of action potentials occurred.

such losses of activation during propagation are not only possible but are also essential for preventing unlimited recruitment of elements. As discussed below, the decrement in $A_{km}$ that occurs as activation propagates is part of what is referred to as *decaying propagation.* A further difference between $x_{ijk}$ and $x_{km}$ elements is that when an $x_{ijk}$ element is activated, the time delay before element $x_{ijk+1}$ is activated is always the same (1 time step, equal to 10 ms). However, for an $x_{km}$ element, the time delay before recruitment is not fixed, but varies as a function of the inputs (discussed below).

Planar array elements are sensitive to *temporal and spatial summation.* This means that the most effective input for an $x_{km}$ element, i.e., the input that results in the largest $A_{km}$ and the smallest delay in $T_{km}$, is to have all $N$ of its inputs arrive at the same time and be as large in magnitude as possible, i.e., $T_{k-1\ m-d} = T_{k-1\ m-d+1} = \ldots = T_{k-1\ m+d}$ and $A_{k-1\ m-d} = A_{k-1\ m-d+1} = \ldots = A_{k-1\ m+d} = \theta_{\text{up}}$, where $\theta_{\text{up}}$ is an upper bound for $A_{km}$ as discussed above. It is assumed that as the temporal/spatial summation of the inputs to element $x_{km}$ increases, $A_{km}$ increases (up to the $\theta_{\text{up}}$ bound). The delay contributing to $T_{km}$ is influenced by a stochastic component so that for a given set of inputs to $x_{km}$, the output time $T_{km}$ is subject to variability. However, the effect of temporal/spatial summation on $T_{km}$ is that the delay in $T_{km}$ tends to decrease to a lower mean value as temporal/spatial summation increases and tends to increase to an upper mean value as temporal/spatial summation decreases. Thus, the effect of temporal/spatial summation is that it allows an element to generate a faster output and one with greater magnitude than an element without this effect.

In the absence of temporal/spatial summation, propagation *decays*, which means that $A_{km}$ decreases and the delay contributing to $T_{km}$ increases as activation progresses to subsequent columns.[15] Note that if only one of the $A_{k-1\ m-d}, \ldots, A_{k-1\ m+d}$ inputs to element $x_{km}$ can be non-zero then that element's output cannot be augmented by temporal/spatial summation. To see the implications of this, refer to Figure 19. Arrows denote activation of

[15] A good physical example of decaying propagation is as follows. Consider a sequence of billiard balls equally spaced in a straight line. Let "activation" of a billiard ball be defined as being struck by either a pool cue or another ball. Let $A_k$ denote the magnitude of activation, i.e., the force with which ball $k$ is struck, and let $T_k$ be the time at which ball $k$ is struck. If one were to strike a ball at one end and begin propagation of activation, propagation would immediately decay, i.e., $A_k$ would decrease and the delay in $T_k$ would increase as the balls activated each other in sequence. To include a stochastic component in this physical analogy, imagine that the surface beneath the balls is randomly smoother in some places and rougher in others; such variations in surface would unpredictably affect the travel time between balls and thus, randomly influence $T_k$. To complete the analogy, temporal/spatial summation for ball $k$ would be like having not only ball $k-1$ strike it, but also having one or more additional balls striking it simultaneously. If each of the balls in the sequence received such temporal/spatial summation, decay would be reduced or eliminated.

positive magnitude, i.e., $A_{km} > 0$. Although the fan-out factor is constant for all elements, the net input for elements lying along the edges of this wave of activation is different from those elements that are located within the interior of the activation wave, i.e., edge elements (which have dots in their centers) receive only one non-zero input while interior elements receive three non-zero inputs.

Thus, because edge elements receive only one active input and thereby never receive temporal/spatial summation, propagation always decays for the edge elements. For example, referring to Figure 19 and temporarily adopting the convention that $A_b$ refers to the activation magnitude of element $b$ and $T_b$ refers to the time of activation of element $b$, when edge element $b$ activates edge element $c$, $A_c < A_b$; in addition, it is likely that $(T_c - T_b) > (T_b - T_a)$.

As a result of the assumptions of planar architecture, convergence and divergence of activation, temporal and spatial summation, and random variation in $T_{km}$, the stimulus trace exhibits the following dynamics.

1. At CS onset there is rapid initial recruitment of elements due to fan-out, a process referred to as *spreading activation.*

2. Spreading activation does not continue indefinitely due to the decaying propagation of the edge elements.

3. Interior elements, which receive temporal/spatial summation, initially propagate with little or no decay. However the decaying propagation of the edge elements progressively affects the temporal/spatial summation of the adjacent interior elements so that ultimately all interior elements decay.

4. The stochastic influence over $T_{km}$ results in variability in output times of the elements and thereby affects temporal summation. This has the effect of producing intertrial variability in the number of elements that are activated at a given time, especially at the upper range of time intervals. Thus, on occasional trials, elements continue to be activated after long intervals; in conditioning simulations this property would make CRs at long ISIs possible (though very slow to develop).

As illustrated below in simulations, these stimulus trace dynamics generate the desired inverted-U-shaped ISI function. The initial rising portion of the function corresponds to the rapid recruitment of elements during spreading activation. The peak of the ISI function occurs when the number of activated elements is at maximum. The falling phase of the ISI function results from the decaying propagation of interior as well as edge elements.

### 3.2 Simulations

This section is intended to suggest how a stimulus trace produced by the dynamics of the planar array architecture can give rise to both CR generation and ISI effects. Because the planar array approach is an extension of the trace described in Section 2, the planar array trace should be capable of simulating the full range of conditioning phenomena described in Section 2 without the need for an $\bar{x}_{ij}(t)$ term. Such simulations are planned and will be the subject of a future report.

Figure 21 illustrates the state of a planar array stimulus trace at four different times after the trace process is initiated. Equations governing this and subsequent simulations are included in the Appendix.[16] The figure depicts the state of the trace at $t = 250$ ms (upper left), $t = 750$ ms (upper right), $t = 1250$ ms (lower left), and $t = 1750$ ms (lower right) after CS onset (at $t = 0$). As in Figure 19, CS input enters at the left edge of the planar array and activation of the elements propagates to the right. In order to graphically present the simulation results, an $x_{km}$ element is assumed to be *effectively on* at $T_{km}$ only if $A_{km} \geq \theta_{\text{on}}$, where $\theta_{\text{on}}$ is an onset threshold of activation ($\theta_{\text{on}} < \theta_{\text{up}}$). As in Section 2, once an $x_{km}$ element is turned on at $T_{km}$, it is assumed to remain on for 100 ms. Thus, for each element at any time $t$,

$$x_{km}(t) = \begin{cases} \text{on} & \text{if } A_{km} \geq \theta_{\text{on}}, \text{ and } t - 100 \leq T_{km} \leq t; \\ \text{off} & \text{otherwise,} \end{cases} \tag{10}$$

where $t = 0$ at CS onset. The dots in the figure represent elements that are currently off and have never been on, the open circles represent elements that are currently off but were previously on, and the filled circles represent elements that are currently on. In a conditioning simulation, the latter elements would be the ones most eligible for modification.[17]

The main point of Figure 21 is that under this model of spreading activation the number of elements that are highly eligible for synaptic modification increases and then decreases over time. This point is further illustrated in Figure 22, which depicts the number of highly eligible (filled-circle) elements as a function of time since CS onset, averaged over 25 trials. The inverted-U shape of this function is similar to interstimulus interval functions obtained

[16] Simulations were conducted by setting $T_{km} = 0$ for all elements and $A_{km} = 0$ for all elements except five in the first column, which were set at $\theta_{\text{up}}$. Beginning with the second column and progressing to the last column, $A_{km}$ and $T_{km}$ were computed for all elements, using equations specified in the Appendix. It was then possible to specify $x_{km}(t)$ at discrete time steps using Equation (10).

[17] In terms of the network model previously described, the filled-circle elements would have larger values of $h_{ijk}(t)$ than the open-circle elements.

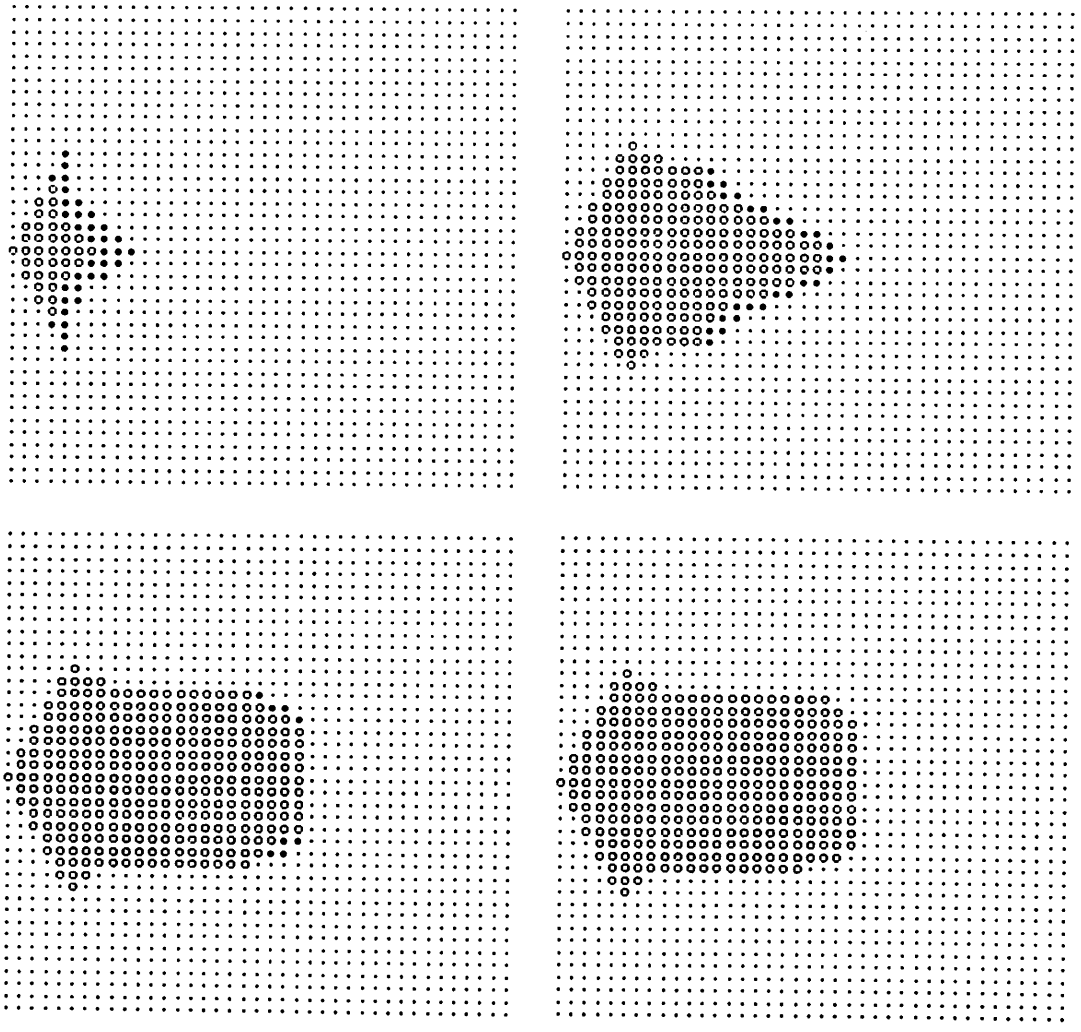

**Figure 21:** Spreading activation in a planar array of elements at four different times after CS onset during a single trial. Details are described in the text. The simulation was conducted using a 200 × 200 array of elements. For illustration purposes, every fifth element is displayed. **Upper left:** $t = 250$ ms after CS onset. **Upper right:** $t = 750$ ms after CS onset. **Lower left:** $t = 1250$ ms after CS onset. **Lower right:** $t = 1750$ ms after CS onset.

from rabbit nictitating membrane experiments (Gormezano, 1972; Gormezano et al., 1983; Schneiderman and Gormezano, 1964; Schneiderman, 1966; Smith, 1968).[18]

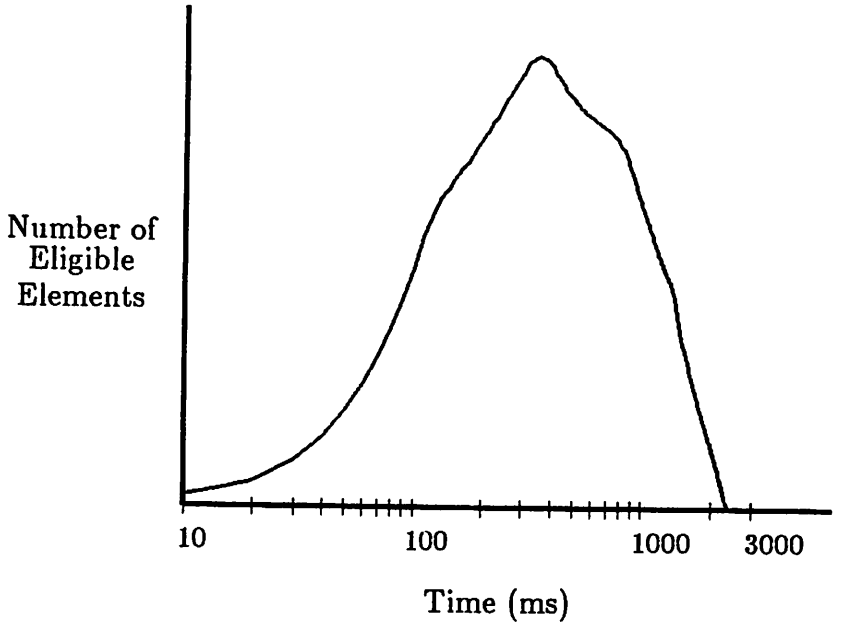


**Figure 22:** Number of eligible elements as a function of time after CS onset (log scale), averaged over 25 trials. "Eligible" here is defined as having being in the *on* state as defined above (same as in Figure 21 for the filled circles).

Figure 23 illustrates how the stochastic component in the calculation of $T_{km}$ can produce intertrial variability in the patterns of activation. This figure depicts the state of the trace at 1750 ms on a trial different from the one depicted in Figure 21. Although the same simulation parameters were used to generate both figures, there are no highly-eligible elements at 1750 ms in Figure 21, but there are quite a few in Figure 23.

[18]In behavioral experiments with the rabbit nictitating membrane response using a tone CS, no evidence of learning is observed with ISI's less than 67 ms (Salafia et al., 1980). This limit is probably due to neuronal recruitment in primary auditory structures, because Patterson (1970) demonstrated that by using electrical stimulation of the inferior colliculus as a CS and thereby bypassing lower auditory structures, robust learning was observed at a 50 ms ISI. In the simulations that generated Figure 22 spreading activation began at CS onset. Thus, to make the simulation more consistent with behavioral data one could delay the onset of spreading activation and thereby shift the ISI curve to the right, and/or assume that a minimum number of elements are necessary before a CR emerges above baseline level.

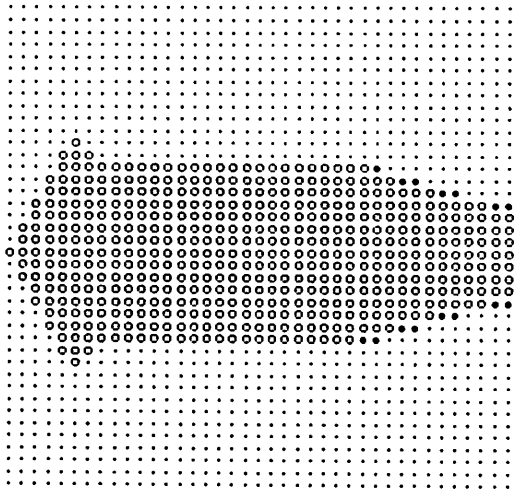

**Figure 23:** State of stimulus trace at 1750 ms after CS onset. The results on this trial are different from the results depicted in Figure 21 at 1750 ms, even though the same simulation parameters were used. The stochastic influence over $T_{km}$ produces *intertrial* variability in the stimulus trace. This allows the trace to provide, on some trials, eligible elements at very long ISIs.

### 3.3 Generalization

An immediate consequence of representing the stimulus trace in the manner outlined above is that generalized responding to similar CSs is now possible. How generalization would occur is illustrated in Figure 24. If the stimulus designated CS represents, for example, a 1000 Hz tone, CS′ might represent a tone of 600 Hz. The figure illustrates that when spreading activation is initiated at the points designated by the CS and CS′ arrows, there is overlap of activated elements; these overlapping elements are depicted as filled circles. Any associative strength that develops in the latter elements from reinforced CS presentations would mediate generalized responding when CS′ is presented.

Suppose that on alternate trials, one stimulus was reinforced and the other stimulus was not (CS+/CS′–), i.e., a *discrimination* paradigm. The overlapping elements would mediate differential responding in the following manner. Let **O** represent the set of overlapping elements for CS and CS′ and let **N** represent the set of non-overlapping elements that are activated by CS′. On CS+ trials, the **O** elements will be reinforced, and on CS′– trials, both **O** and **N** elements will not be reinforced. Thus, the pattern of **O**+ / **ON**– constitutes conditioned inhibition training for the **N** elements. On CS′ trials the inhibitory weights of

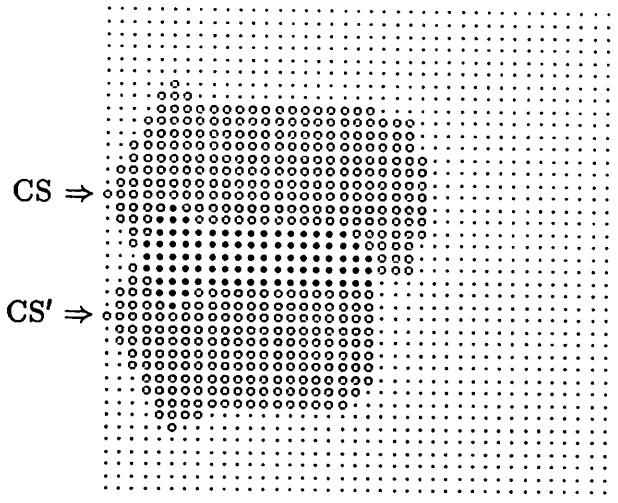


**Figure 24:** Stimulus generalization brought about through overlapping activation of stimulus trace elements. CS and CS′ denote similar CSs of the same modality. Two trials were simulated to generate this figure. The only difference in the two trials was the point of CS initiation (see CS and CS′ arrows). In this figure, open circles represent elements that were turned on once during the two trials, filled circles are elements that were turned on twice, and dots represent elements that never turned on during either trial.

the N elements will cancel the excitatory weights of the O elements and the CR will be suppressed.

Note that CSs of different stimulus modalities are assumed to propagate on different planar arrays of elements. For example, presentation of a light CS would not activate any of the elements in Figure 24 because these elements would be "dedicated" to auditory CSs. Thus, cross-modal generalization would not occur (Moore, 1972).

## 4. Concluding remarks

Philosophers as early as Aristotle hypothesized that associations between events occur according to some Law of Contiguity (see Gormezano and Kehoe, 1981, for a review). In its simplest form, this law states that a connection between two events will form if they occur in spatiotemporal proximity to one another. In light of the fact that the ultimate form of temporal proximity is simultaneity, Pavlov's discovery of robust learning under a trace conditioning paradigm and poor learning with simultaneous CS–US pairings posed a challenge to contiguity theorists. As a result, the stimulus trace was proposed as a mechanism to bridge the gap between nominal CSs and USs, thus preserving the notion of simultaneity as the basis of learned association.

Recently, intracellular physiological experiments have begun to address the issue of temporal contiguity in learning (Kelso et al., 1986; Wigström et al., 1986). In these experiments, simultaneous pre- and postsynaptic stimulation resulted in enhanced synaptic responses. However, asynchronous activations (amounting to delay conditioning protocols with ISIs of 210 and 420 ms) failed to produce synaptic enhancement. Thus, although intracellular mechanisms have been proposed to account for ISI effects on conditioning (Gingrich and Byrne, 1987), neurophysiological studies to date support the view that simultaneous occurrence of events produces optimal association.

The network model presented in Section 2, with the implementation of the spreading activation stimulus trace of Section 3, offers a framework in which simultaneity is the underlying mechanism for learning at the "atomic" level, and yet asynchronous CS–US pairing produces the most robust demonstrations of learning at the system output (behavioral) level. At the network's atomic level, changes in a synaptic $V_{ijk}$ weight occur in proportion to the eligibility of the synapse $[h_{ijk}(t)]$. This eligibility is maximal when the $x_{ijk}$ element is first activated, and thus, simultaneous activation of an $x_{ijk}$ element with the US produces the greatest change in weight.

Although simultaneity is optimal for learning *at the synapse*, simultaneous CS–US presentation is not optimal at the system output level, where learning is measured by the magnitude of CRs and the rate at which CRs develop. The latter characteristics are a function of the *total number of synapses that contribute to the output*, and this number in turn depends upon the number of synapses that are eligible when the US occurs. Section 3 showed that with a spreading activation mechanism, the number of eligible synapses changes as a function of time. Inspection of Figure 22 reveals that relatively few synapses are eligible at extremely short interstimulus intervals. Thus, with simultaneous CS–US pairings, the number of elements contributing to the output are too few to have

any appreciable effect.

This report began with a discussion of two fundamental phenomena of classical conditioning: The anticipatory nature of conditioned responses and the effect of the interstimulus interval on the rate of conditioning. Although both of these phenomena do not necessarily have to arise from a single trace mechanism, as has been assumed by some learning theorists, the simulations presented in this report show how one type of network organization can model both CR-generating and rate-governing functions of the trace, with each function emerging independently of the other. Section 2 demonstrated that anticipatory CRs can be generated by virtue of the forward propagation of elements in a simple (one-dimensional) tapped delay-line trace, such as those depicted in Figures 5 and 6. This trace architecture is sufficient for simulating basic temporal properties of CRs observed in experimental studies of conditioning, including decreasing onset latency during acquisition training, peak amplitude occurring at the temporal locus of the US, inhibition of delay, and trace conditioning. It was further argued in Section 3 that by expanding the dimensionality of the trace architecture and implementing rules for spreading activation, the recruitment of elements during propagation can model ISI effects and stimulus generalization.

In designing the network model, efforts were made to keep assumptions as simple as possible and consistent with known neurobiological principals in order to retain some degree of neural plausibility. Well-documented neurobiological concepts such as convergence and divergence (fan-in and fan-out), and spatial and temporal summation were used to model spreading activation (although the representation no doubt oversimplifies actual neuron behavior). As for the presence of tapped delay-line architectures in the nervous system, researchers have noted such architectural arrangements in brain structures such as the reticular formation (Scheibel and Scheibel, 1958; 1967) and cerebellar cortex (Braitenberg, 1967; Freeman, 1969; Kent, 1981), and have speculated upon their possible timing functions. However, whether or not the nervous system actually uses such architectures to generate adaptively timed responses is an open question.

## Acknowledgements

This research was supported by AFOSR grant 86-0182. The author wishes to thank J.W. Moore and D.E.J. Blazis for helpful comments and discussions.

# A. Appendix: The planar array stimulus trace

The equations describing how $A_{km}$, the output activation of the element in the $k^{\text{th}}$ column and $m^{\text{th}}$ row, is calculated are as follows:

$$A_{km} = c(1 + \Upsilon_{km})A^{\text{in}}_{\text{max}}, \tag{11}$$

where $c$ is a constant ($0 < c < 1$) that governs the amount of decay in activation from input to output. $A^{\text{in}}_{\text{max}}$ is the maximum input activation to element $x_{km}$, i.e., $A^{\text{in}}_{\text{max}} = \max\{A_{k-1\ m-d}, \ldots, A_{k-1\ m+d}\}$. $A_{km}$ is limited by an upper bound, $\theta_{\text{up}}$ (where $\theta_{\text{up}} > 0$) so that $0 \leq A_{km} \leq \theta_{\text{up}}$. $\Upsilon_{km}$ represents temporal and spatial summation of the inputs and is defined as:

$$\Upsilon_{km} = \frac{\sum_{p=m-d}^{m+d-1} \sum_{r=p+1}^{m+d} A_{k-1\ p}\, A_{k-1\ r}\ e^{-|T_{k-1\ p} - T_{k-1\ r}|}}{\theta^2_{\text{up}} \binom{N}{2}} \tag{12}$$

where $N$ is the fan-out factor ($N = 2d + 1$, where $d$ is a positive integer). The term $\binom{N}{2}$ denotes the number of combinations of $N$ taken 2 at a time.

In calculating the effects of temporal and spatial summation, $\Upsilon_{km}$, in Equation (12), all possible products between pairs of input activations are summed, and each product is weighted by the temporal separation of the two inputs. For $N$ inputs there are $\binom{N}{2}$ possible pairs of products. If the activation of each input is at maximum, i.e., $A_{k-1\ m-d} = A_{k-1\ m-d+1} = \ldots = A_{k-1\ m+d} = \theta_{\text{up}}$, and all inputs arrive at the same time, the numerator of Equation (12) becomes $\sum_p \sum_r \theta_{\text{up}}\theta_{\text{up}}e^0 = \theta^2_{\text{up}}\binom{N}{2}$, and thus, $\Upsilon_{km} = 1$. At the other extreme, if only one (or none) of the inputs have activation magnitude greater than zero, then the cross-product term is zero and $\Upsilon_{km} = 0$.

Substituting these possible values of $\Upsilon_{km}$ into Equation (11), one finds that $A_{km}$can range from a minimum value of $cA^{\text{in}}_{\text{max}}$ when $\Upsilon_{km} = 0$ to a maximum value of $2cA^{\text{in}}_{\text{max}}$ when $\Upsilon_{km} = 1$. Consider the elements on the edges of the spreading activation, for which $\Upsilon_{km} = 0$ is always true (because edge elements can have only one non-zero input), and thus, $A_{km} = cA^{\text{in}}_{\text{max}}$. Because $c < 1$, $A_{km} < A^{\text{in}}_{\text{max}}$ is always true, i.e., output is less than maximum input. Thus, because $A_{km}$ for an edge element in a given layer constitutes the $A^{\text{in}}_{\text{max}}$ for the edge element in the next layer, and because $A_{km}$ decreases with each successive activation, activation decays with propagation for the edge elements, as discussed in Section 3.

Now consider the interior elements, for which $\Upsilon_{km}$ can take values greater than zero.[19] By algebraic manipulation of Equation (11), $A_{km} < A^{\text{in}}_{\max}$ is true only when $\Upsilon_{km} < \frac{1}{c} - 1$. When $\Upsilon_{km} \geq \frac{1}{c} - 1$, output of an element can be greater than or equal to its maximum input. Thus, activation does not decay with propagation for the interior elements as long as spatial/temporal summation remains sufficiently strong.

The next two equations describe how $T_{km}$ is calculated. The expression for $T_{km}$ is

$$T_{km} = \bar{T}^{\text{in}}_{km} + \mathcal{N}(\mu, \sigma), \tag{13}$$

where $\bar{T}^{\text{in}}_{km}$ is a weighted mean of the input times, i.e., $\bar{T}^{\text{in}}_{km} = \sum_{p=m-d}^{m+d} T_{k-1\ p} A_{k-1\ p} / \sum_p A_{k-1\ p}$ ($\bar{T}^{\text{in}}_{km} = 0$ if $\sum_p A_p = 0$). $\mathcal{N}(\mu, \sigma)$ is a random variable sampled from a normal distribution of mean $\mu$ and standard deviation $\sigma$, where $\mu$ is determined by the equation:

$$\mu = \mu_{\min} + (\mu_{\max} - \mu_{\min}) \left(1 - \frac{A_{km}}{\theta_{\text{up}}}\right), \tag{14}$$

where $\mu_{\min}$ and $\mu_{\max}$ are constants that determine the minimum and maximum possible values that $\mu$ can take.

Equation (13) states that the output time for an element is determined by the mean time of its inputs ($\bar{T}^{\text{in}}_{km}$) plus some additional delay [$\mathcal{N}(\mu, \sigma)$]. The latter component is a random variable whose expected value is determined by the magnitude of activation of the element. For example, in Equation (14) it is evident that when $A_{km}$ is equal to its upper threshold, $\theta_{\text{up}}$, the term $A_{km}/\theta_{\text{up}}$ becomes equal to 1 and $\mu = \mu_{\min}$. Thus, $T_{km}$ is likely to be small when $A_{km}$ is large. However, as $A_{km}$ approaches zero, $\mu$ approaches $\mu_{\max}$ and $T_{km}$ is likely to be large. The standard deviation, $\sigma$ in Equation (13), is a constant.

Simulations were conducted using a 200 × 200 array of elements. At the start of the simulation, $T_{km} = 0$ for all elements and $A_{km} = 0$ for all elements except 5 in the first column. The latter elements had $A_{km} = \theta_{\text{up}}$. Beginning with column 2 and proceeding to the last column, $A_{km}$ then $T_{km}$ was calculated for each element in the column, beginning with row $d + 1$ and ending with row $200 - d - 1$. ($d$ was defined above. $A_{km}$ and $T_{km}$ cannot be calculated for rows less that $d + 1$ or greater than $200 - d - 1$, so $A_{km}$ and $T_{km}$ for elements in these rows remain at 0 during the simulation.)

Simulation parameters for Figures 21, 22, 23 and 24 were: $c = 0.9$, $\theta_{\text{up}} = 100$, $\theta_{\text{on}} = 10$, fan-out factor $= 5$, $\sigma = 0.3$, $\mu_{\min} = 4$, $\mu_{\max} = 16$.

[19] This is almost always true, the one exception being the element in the middle row and middle column of Figure 19, which receives only one non-zero input.

## References


Barto, A. G., & Sutton, R. S. (1982). Simulation of anticipatory responses in classical conditioning by a neuron-like adaptive element. *Behavioural Brain Research, 4*, 221-235.

Blazis, D. E. J., & Moore, J. W. (1987). Simulation of a classically conditioned response: components of the input trace and a cerebellar neural network implementation of the Sutton-Barto-Desmond model. Technical Report 87-74.

Boneau, C. A. (1958). The interstimulus interval and the latency of the conditioned eyelid response. *Journal of Experimental Psychology, 56*, 464-472.

Braitenberg, V. (1967). Is the cerebellar cortex a biological clock in the millisecond range? In C. A. Fox & R. S. Snider (Eds.), *Progress in Brain Research Vol. 25. The Cerebellum* (pp. 334-346). New York: Elsevier Publishing Company.

Coleman, S. R., & Gormezano, I. (1971). Classical conditioning of the rabbit's (*Oryctolagus cuniculus*) nictitating membrane response under symmetrical CS–US interval shifts. *Journal of Comparative and Physiological Psychology, 77*, 447-455.

Desmond, J. E., Blazis, D. E. J., Moore, J. W., & Berthier, N. E. (1986). Computer simulations of a classically conditioned response using neuron-like adaptive elements: Response topography. *Society for Neuroscience Abstracts, 12*, 516.

Desmond, J. E., & Moore, J. W. (1988). Adaptive timing in neural networks: The conditioned response. *Biological Cybernetics, 58*, 405-415.

Freeman, J. A. (1969). The cerebellum as a timing device: An experimental study in the frog. In R. Llinas (Ed.), *Neurobiology of Cerebellar Evolution and Development* (pp. 397-420). Chicago: American Medical Association.

Gelperin, A., Hopfield, J. J., & Tank, D. W. (1985). The logic of *Limax* learning. In A. Selverston (Ed.), *Model Neural Networks and Behavior*. New York: Plenum Press.

Gingrich, K. J., & Byrne, J. H. (1987). Single-cell neuronal model for associative learning. *Journal of Neurophysiology, 57*, 1705-1715.

Gluck, M. A., & Bower, G. H. (1988). Evaluating an adaptive network model of human learning. *Journal of Memory and Language, 27*, 166-195.

Gluck, M. A., & Thompson, R. F. (1987). Modeling the neural substrates of associative learning and memory: A computational approach. *Psychological Review, 94*, 176-191.

Gormezano, I. (1972). Investigations of defense and reward conditioning in the rabbit. In A. H. Black & W. F. Prokasy (Eds.), *Classical Conditioning II: Current Research and Theory* (pp. 151-181). New York: Appleton–Century–Crofts.

Gormezano, I., & Kehoe, E. J. (1981). Classical conditioning and the Law of Contiguity. In P. Harzem & M. D. Zeiler (Eds.), *Predictability, Correlation, and Contiguity* (pp. 1-45). New York: John Wiley & Sons Ltd.

Gormezano, I., Kehoe, E. J., & Marshall, B. S. (1983). Twenty years of classical conditioning with the rabbit. *Progress in Psychobiology and Physiological Psychology, 10*, 197-275.

Gormezano, I., & Moore, J. W. (1969). Classical conditioning. In M. H. Marx (Ed.), *Learning: Processes.* London: Collier-Macmillan Limited.

Grossberg, S., & Schmajuk, N. A. (1987). Neural dynamics of attentionally modulated Pavlovian conditioning: Conditioned reinforcement, inhibition, and opponent processing. *Psychobiology, 15*, 195-240.

Hebb, D. O. (1949). *The Organization of Behavior.* New York: Wiley.

Hull, C. L. (1943). *Principles of Behavior.* New York: Appleton–Century–Crofts.

Hull, C. L. (1952). *A Behavior System.* New Haven, Connecticut: Yale University Press.

Kamin, L. J. (1968). Attention-like processes in classical conditioning. In W. F. Prokasy (Ed.), *Classical conditioning: A symposium* (pp. 118-147). New York: Appleton.

Kelso, S. R., Ganong, A. H., & Brown, T. H. (1986). Hebbian synapses in hippocampus. *Proceedings of the National Academy of Science (USA), 83*, 5326-5330.

Kent, E. W. (1981). *The brains of men and machines.* Peterborough, NH: BYTE/McGraw Hill.

Klopf, A. H. (1972). Brain function and adaptive systems– A heterostatic theory. Technical Rep. No. 133 [AFCRL-72-0164]. Air Force Cambridge Research Laboratories. L. G. Hanscom Field, Bedford, Massachusetts.

Klopf, A. H. (1986). A drive reinforcement model of single neuron function: An alternative to the Hebbian neural model. In J. S. Denker (Ed.), *Neural Networks for Computing, AIP Conference Proceedings 151.* New York: American Institute of Physics.

Klopf, A. H. (1988). A neuronal model of classical conditioning. *Psychobiology, 16,* 85-125.

Leonard, D. W., & Theios, J. (1967). Effect of CS–US interval shift on classical conditioning of the nictitating membrane in the rabbit. *Journal of Comparative and Physiological Psychology, 63,* 355-358.

Levine, D. S. (1986). A neural network model of temporal order effects in classical conditioning. In J. Eisenfeld & M. Witten (Eds.), *Modelling of Biomedical Systems.* North-Holland: Elsevier Science Publishers B.V.

Logan, F. A. (1956). A micromolar approach to behavior theory. *Psychological Review, 65,* 63-73.

Marchant, H. G. III, Mis, F. W., & Moore, J. W. (1972). Conditioned inhibition of the rabbit's nictitating membrane response. *Journal of Experimental Psychology, 95,* 408-411.

Marchant, H. G. III, & Moore, J. W. (1973). Blocking of the rabbit's conditioned nictitating membrane response in Kamin's two-stage paradigm. *Journal of Experimental Psychology, 101,* 155-158.

Millenson, J. R., Kehoe, E. J., & Gormezano, I. (1977). Classical conditioning of the rabbit's nictitating membrane response under fixed and mixed CS–US intervals. *Learning and Motivation, 8,* 351-366.

Moore, J. W. (1972). Stimulus control: Studies of auditory generalization in rabbits. In A. H. Black & W. F. Prokasy (Eds.), *Classical Conditioning II. Current Theory and Research.* New York: Appleton-Century-Crofts.

Moore, J. W., & Blazis, D. E. J. (in press). Cerebellar implementation of a computational model of classical conditioning. In P. Strata (Ed.), *Proceedings of the Satellite Symposium of the 2nd IBRO World Congress of Neuroscience: The olivocerebellar system in motor control.* New York: Springer-Verlag.

Moore, J. W., Desmond, J. E., Berthier, N. E., Blazis, D. E. J., Sutton, R. S., & Barto, A. G. (1986). Simulation of the classically conditioned nictitating membrane response by a neuron-like adaptive element: Response topography, neuronal firing, and interstimulus intervals. *Behavioural Brain Research, 21*, 143-154.

Patterson, M. M. (1970). Classical conditioning of the rabbit's (*Oryctolagus cuniculus*) nictitating membrane response with fluctuating ISI and intracranial CS. *Journal of Comparative and Physiological Psychology, 72*, 193-202.

Pavlov, I. P. (1927). *Conditioned Reflexes (Translated by G.V. Anrep).* New York: Dover Publications, Inc.

Rescorla, R. A. (1969). Pavlovian conditioned inhibition. *Psychological Bulletin, 72*, 77-94.

Rescorla, R. A., & Wagner, A. R. (1972). A theory of Pavlovian conditioning: Variations in the effectiveness of reinforcement and nonreinforcement. In A. H. Black & W. F. Prokasy (Eds.), *Classical Conditioning II: Current Theory and Research.* New York: Appleton-Century-Crofts.

Salafia, W. R., Lambert, R. W., Host, K. C., Chiaia, N. L., & Ramirez, J. J. (1980). Rabbit nictitating membrane conditioning: Lower limit of effective interstimulus interval. *Animal Learning and Behavior, 8*, 85-91.

Scheibel, M. E., & Scheibel, A. B. (1958). Structural substrates for integrative patterns in the brain stem reticular core. In H. Jasper, L. D. Proctor, R. S. Knighton, W. S. Noshay, & R. T. Costello (Eds.), *Reticular Formation of the Brain* (pp. 31-55). Boston: Little, Brown.

Scheibel, M. E., & Scheibel, A. B. (1967). Anatomical basis of attention mechanisms in vertebrate brains. In G. C. Quarton, T. Melnechuk, & F. O. Schmitt (Eds.), *The Neurosciences. A Study Program* (pp. 577-602). New York: The Rockefeller University Press.

Schmajuk, N. A., & Moore, J. W. (1985). Real-time attentional models for classical conditioning and the hippocampus. *Physiological Psychology, 13*, 278-290.

Schmajuk, N. A., & Moore, J. W. (1988). The hippocampus and the classically conditioned nictitating membrane response: A real-time attentional-associative model. *Psychobiology, 16*, 20-35.

Schneiderman, N. (1966). Interstimulus interval function of the nictitating membrane response in the rabbit under delay versus trace conditioning. *Journal of Comparative and Physiological Psychology, 62*, 397-402.

Schneiderman, N., & Gormezano, I. (1964). Conditioning of the nictitating membrane of the rabbit as a function of CS–US interval. *Journal of Comparative and Physiological Psychology, 57*, 188-195.

Smith, M. C. (1968). CS–US interval and US intensity in classical conditioning of the rabbit's nictitating membrane response. *Journal of Comparative and Physiological Psychology, 66*, 679-687.

Sutton, R. S., & Barto, A. G. (1981). Toward a modern theory of adaptive networks: Expectation and prediction. *Psychological Review, 88*, 135-170.

Tesauro, G. (1986). Simple neural models of classical conditioning. *Biological Cybernetics, 55*, 187-200.

Wagner, A. R. (1981). SOP: A model of automatic memory processing in animal behavior. In N. E. Spear & R. R. Miller (Eds.), *Information Processing in Animals: Memory Mechanisms.* Hillsdale, NJ: Erlbaum.

Wigström, H., Gustafsson, B., Huang, Y. Y., & Abraham, W. C. (1986). Hippocampal long-term potentiation is induced by pairing single afferent volleys with intracellularly injected depolarizing current pulses. *Acta Physiologica Scandinavica, 126*, 317-319.